

**Thesis to reach the degree of an
MASTER OF ENGINEERING**

from Benjamin Mayer

born on the 17.04.1990 in Leipzig

TITLE:

**LABORATORY STUDIES OF THE PYROLYSIS OF ORGANIC
WASTES FOR OBTAINING USEFUL PRODUCTS**

Supervisors: Prof. Dr.-Ing. Dietmar Heinz

M.Eng. Felix Steininger

Prof. Dr. Albina Ribeiro

Merseburg, 29.09.2017

ACKNOWLEDGEMENT

Thanks to Prof. Albina Ribeiro, Eng. Ana Almeida, Eng. Vânia Silva and everybody else from CIETI for supporting, supervising and helping me.

Thanks to the entire laboratory staff from ISEP, especially Eng. Aurora Silva and Eng. Paula Venda, for supervising me in the laboratories.

I also want to thank Prof. Dietmar Heinz for supervision and Cornelia Lorenz for supporting me with Erasmus questions.

STATEMENT OF AUTHORSHIP

I declare to have authored this work on my own, without any other than the indicated means.

ABSTRACT

This work investigated the influence of different set-point temperatures from 550 °C to 950 °C on the performance of the pyrolysis process of mesocarp oil palm fibre (OPF). The experiments were performed in a fixed bed reactor with a length of 780 mm and an inner diameter of 97 mm, with a split furnace; the temperature difference between the experiments was 100 °C. For all the experiments, the heating rate was set to 20 °C·min⁻¹ and the fixed N₂ flow rate of 2.463 g·min⁻¹ was used. To assess pyrolysis performance, the yields of each phase were determined and its products were characterized.

The results show, that the char yield slightly decreased with the increase of temperature, while the liquid yield had its maximum at a set-point temperature of 850 °C. The gas yield was calculated by mass difference. The higher heating value (HHV) of the char and the liquid was nearly constant around 28 MJ·kg⁻¹, and only in the liquid phase the value dropped at a set-point temperature of 850 °C. The HHV of the gas phase increased with rising temperature and the maximum obtained value was 2.2 MJ·(Nm³)⁻¹.

Regarding char properties, with increasing temperature, the fixed carbon content in the char increased until a temperature of 850 °C, and its maximum was 79 %. Its ash content was constant around 12 % for all experiments.

The bio-oil may have several compounds in its composition like carboxylic acid, ketones, aldehydes, alcohols, aromatic, acyl and alkoxy groups that were determined by FTIR.

In the gas composition the production of H₂ increased more than six times along the tested temperatures, with a maximum value of 10.96 mol·(kg OPF)⁻¹, at the highest tested temperature. The CO production increased rapidly with increasing temperature as well. For the CO and CH₄ production the increase was not as high.

This work shows that products obtained from the OPF pyrolysis can be used as energy sources and for obtaining chemicals.

INDEX

List of figures.....	III
List of tables.....	IV
List of symbols.....	V
1. Introduction.....	- 1 -
2. Biomass characterisation.....	- 3 -
2.1. Structure of biomass.....	- 4 -
2.2. Biomass as a fuel.....	- 6 -
2.2.1. Proximate analysis.....	- 7 -
2.2.2. Ultimate analysis.....	- 8 -
2.2.3. Thermogravimetric analysis.....	- 8 -
2.2.4. Heating value.....	- 9 -
2.2.5. Other properties.....	- 12 -
3. Basics of pyrolysis.....	- 13 -
3.1. Influence of temperature on the pyrolysis performance.....	- 13 -
3.2. Influence of heating rate and gas residence time on the pyrolysis performance.....	- 16 -
3.2.1. Fast pyrolysis.....	- 16 -
3.2.2. Slow pyrolysis.....	- 17 -
3.3. Other parameters that influence the pyrolysis performance.....	- 18 -
3.3.1. Chemical composition of the raw material.....	- 18 -
3.3.2. Carrier gas flow rate.....	- 21 -
3.3.3. Physical properties of the raw material.....	- 22 -
3.4. Types of pyrolysis reactors.....	- 22 -
3.4.1. Fixed bed reactors.....	- 23 -
3.4.2. Moving bed reactors.....	- 24 -

4. Pyrolysis of oil palm residues.....	- 31 -
4.1. Introduction	- 31 -
4.2. Literature search	- 32 -
5. Experimental Part	- 37 -
5.1. Characterisation of the raw material.....	- 37 -
5.2. Experimental apparatus.....	- 39 -
5.3. Experimental procedure	- 41 -
6. Results and discussion	- 43 -
6.1. Yields of the pyrolysis products	- 43 -
6.2. Higher heating values of the pyrolysis products	- 44 -
6.3. Gas phase analysis.....	- 46 -
6.4. Char analysis.....	- 48 -
6.5. Liquid phase analysis.....	- 49 -
7. Summary and Conclusions.....	- 51 -
References	- 53 -
Appendix A: Calculations	- 57 -
A.1. Calculation of the gas composition.....	- 57 -
A.2. Treatment of the TG results.....	- 61 -
Appendix B: Ultimate analysis results	- 65 -
Appendix C: Photographs of the reaction system.....	- 67 -

LIST OF FIGURES

Figure 2.1: Typical structure of cellulose.....	- 5 -
Figure 2.2: Molecular structure of hemicellulose, example: xylan	- 5 -
Figure 2.3: Example for lignin structure, beech wood lignin	- 6 -
Figure 2.4: Bases of biomass composition	- 6 -
Figure 3.1: DSC curves of hemicellulose, cellulose and lignin pyrolysis.....	- 21 -
Figure 3.2: Different reactor types: (a) Bubbling bed; (b) Circulating fluidised bed	- 29 -
Figure 5.1: FTIR results of raw material with marked peaks.....	- 38 -
Figure 5.2: Photograph of OPF.	- 39 -
Figure 5.3: Scheme of the reaction system.....	- 40 -
Figure 6.1: Avg. yields of product phases at different avg. inner temperatures.	- 43 -
Figure 6.2: HHVs of the product phases according to the avg. inner temperature. -	44 -
Figure 6.3: Produced gas components according to inner temperature.....	- 46 -
Figure 6.4: Produced gas per kg of raw material according to inner temperature. -	47 -
Figure 6.5: FC, VM and ash of the char at different temperatures.....	- 48 -
Figure 6.6: FTIR results of all experiments.	- 49 -
Figure A.1: Example for different GC-TCD chromatogram.....	- 57 -
Figure A.2: Example of a TG graph, for the char from the 550 °C pyrolysis.....	- 63 -
Figure B.1: Results of the ultimate analysis.....	- 66 -
Figure C.1: Reaction system.....	- 67 -
Figure C.2: Photographs of condensing system.	- 68 -
Figure C.3: Gas analyser (left) and temperature controller(right).....	- 68 -

LIST OF TABLES

Table 2.1: Proximate and ultimate analysis results of different biomasses	- 9 -
Table 5.1: Properties of OPF, comparison with literature	- 37 -
Table 5.2: FTIR results of the raw material.....	- 38 -
Table 6.1: HHV of different fuels	- 45 -
Table 6.2: FTIR results for the charts compared with the literature.....	- 50 -
Table A.1: Density, peak times and calibration curves of gas components.....	- 58 -
Table A.2: Section of TG results, example for char from pyrolysis	- 61 -

LIST OF SYMBOLS

Abbreviations:

(g)	–	gaseous	
(s)	–	solid	
adb	–	air dried basis	
arb	–	as received basis	
avg.	–	average	
db	–	dry basis	
daf	–	dry ash-free basis	
DTG	–	differential thermogravimetric analysis	
EFB	–	empty fruit bunch	
FTIR	–	Fourier transform infrared spectroscopy	
H/C	–	hydrogen to carbon ratio	
HHV	–	higher heating value	[MJ·kg ⁻¹], [kJ·kg ⁻¹] or [MJ·(Nm ³) ⁻¹]
HTC	–	hydrothermal carbonisation	
GC	–	gas chromatograph	
LHV	–	lower heating value	[MJ·kg ⁻¹]
O/C	–	oxygen to carbon ratio	
OPF	–	mesocarp oil palm fibre	
OPFP	–	oil palm fibre pellets	
OPS	–	oil palm shell	
PCK	–	palm kernel shell	
RTP	–	rapid thermal pyrolysis	
TG	–	thermogravimetric analysis	
vol-%	–	volume percentage	
wt-%	–	weight percentage	

Symbols:

A	–	ash content	[wt-%]
A _{H₂}	–	area of hydrogen	[mV·s]
A _{N₂}	–	area of nitrogen	[mV·s]

d_p	–	particle diameter	[mm]
c_{H_2}	–	mass concentration of hydrogen	[mg·mL ⁻¹]
c_{N_2}	–	mass concentration of nitrogen	[mg·mL ⁻¹]
$c_{V_{H_2}}$	–	volume concentration of hydrogen	[vol-%]
$c_{V_{N_2}}$	–	volume concentration of nitrogen	[vol-%]
FC	–	fixed carbon content	[wt-%]
M	–	total moisture content	[wt-%]
M_i	–	inherent moisture content	[wt-%]
M_s	–	surface moisture content	[wt-%]
m_i	–	sample mass at given time	[mg]
m_l	–	mass loss	[mg]
m_M	–	moisture mass	[mg]
m_s	–	initial sample mass	[kg]
m_{VM}	–	mass of volatile matter	[mg]
n_g	–	total number of moles of the entire gas for one bag	[kmol]
n_{H_2}	–	total number of moles of hydrogen for one bag	[kmol]
n_i	–	total number of moles for each component for one bag	[kmol]
$n_{g,total}$	–	total number of moles for the entire gas of all bags	[kmol]
$n_{H_2,total}$	–	total number of moles for hydrogen of all bags	[kmol]
$n_{i,total}$	–	total number of moles for each component of all bags	[kmol]
\dot{n}_j	–	molar flow rate for every component	[kmol·s ⁻¹]
\dot{n}_g	–	molar flow of the entire gas	[kmol·s ⁻¹]
\dot{n}_{H_2}	–	molar flow rate of hydrogen	[kmol·s ⁻¹]
$\dot{n}_{N_2,start}$	–	initial molar flow rate of nitrogen	[kmol·s ⁻¹]
t_{end}	–	end time of gas sample	[min]
T_i	–	temperature inside the sample	[°C]
T_c	–	controlled temperature in the furnace	[°C]
T_{set}	–	set-point temperature	[°C]
t_{start}	–	start time of gas sample	[min]
VM	–	volatile matter content	[wt-%]

Y_g	–	yield of entire gas per kg of raw material	$[\text{kmol} \cdot (\text{kg OPF})^{-1}]$
Y_{H_2}	–	yield of hydrogen per kg of raw material	$[\text{kmol} \cdot (\text{kg OPF})^{-1}]$
Greek letters:			
ρ_{H_2}	–	density of hydrogen at 20 °C and 1 bar	$[\text{mg} \cdot (\text{cm}^3)^{-1}]$
ρ_{N_2}	–	density of nitrogen at 20 °C and 1 bar	$[\text{mg} \cdot (\text{cm}^3)^{-1}]$

1. INTRODUCTION

All around the globe humanity needs fuel, not only now but also in the future. Fossil fuels are the main contributor of energy so far, but they are not inexhaustible and therefore their price rises. They also give a main credit of greenhouse gases, which influence the climate on the planet. The release of CO₂ from fossil fuels is a problem, because the CO₂ is stored in the fuels over centuries and is set free in a much shorter period of time. Therefore the research for alternative and sustainable fuel and energy resources gains interest, not only in environmental but also in economic aspects in the last decades. Biomass is one of the most promising alternatives, because it is renewable and mostly a by-product of already established processes. On the other hand, it is difficult to store, transport and utilize in its original form due to its high moisture content (M), low grinding ability, low bulk and energy densities and its non-uniform shape and size /1, p.569/. Therefore it is important to know the biological, chemical and physical properties, not only from the biomass itself, but for the whole provision chain from its origins to its final conversion to primary or secondary energy. In 2014 the worldwide energy demand was 602 EJ and it is expected to grow in the future. Biomass has a worldwide theoretical potential 159.7 EJ without the usage of energy crops. The highest amount of this potential has woody biomass with 108.4 EJ. In Europe, America and Africa its percentage is above 70 % of the whole biomass potential, only in Asia it has around 40 %, while stalk material makes up 50 % of the biomass potential. The worldwide technical potential of biomass including energy crops is 363.3 EJ (2014) but its actual usage is only 21 % of the technical potential. Therefore it is relevant to improve the usage of biomass as an energy distributor, because with an efficient usage of biomass it could make up more than half of the world's energy demand. The usage of biomass varies with regional influences, for example, the energy demand of Africa and South America could be covered with their technical biomass potential. North America, Europe and Asia have a much higher demand than their biomass potential. Until today 80 % of energy from biomass is used for providing heat, 10 % are used for electricity and the other 10 % are used as fuels /2, p.9–24/.

Fuels from biomass can be acquired through thermo-chemical conversion processes like pyrolysis or gasification. Pyrolysis delivers gaseous, solid and liquid products, which have different utilities, for example, as secondary fuels. The release of CO₂ from biomass fuels has a much lower influence on the earth atmosphere because the CO₂ is stored over a much shorter period of time.

The main objective of this work was to investigate the influence of different temperatures on the pyrolysis process of the (OPF). An overview of the yields and usefulness of its products is also provided.

The work is divided in seven chapters. Chapter two describes the characterisation of biomass in structure and as a fuel. It gives an overview of the different methods of analyses. The third chapter talks about pyrolysis itself, important process parameters, that define different pyrolysis types, and their influence on the process. It also gives an overview of different reactor types and their use. In the fourth chapter there is an overview of previous work of OPF pyrolysis. Chapter five describes the experimental set up of the pyrolysis system and the different analysis for the products and the raw material. The sixth chapter shows and discusses the results of the experiments and the chapter seven gives a summary, conclusions and suggestions for future work.

2. BIOMASS CHARACTERISATION

Biomass is any biodegradable organic matter from dead or alive living beings, including their wastes, products and residues that are non-fossilised. Energy produced from biomass is called greenhouse gas neutral because the CO₂ released during its degradation was stored in the recent past in comparison to fossil fuel that stored CO₂ over centuries. Biomass can be differentiated into three categories, depending on their origin. Primary biomass is organic matter that is directly formed under the effect of photosynthesis from sunlight, like the whole flora, its by-products and wastes. Secondary biomass is all organic matter that is produced by the conversion and decomposition of primary biomass in higher living beings, like animals, including their by-products and wastes. Tertiary biomass is organic matter that is processed in at least one technical step from primary or secondary biomass, for example pulp or cotton clothing /2, p.3/ 3, p.27/. Biomass has different potentials that give restrictions on its usage:

- **The theoretical potential** is the temporary, local and theoretically physical usable offer of energy. It is restricted by technical, environmental, structural, statutory and social limitations, so it is not relevant for the practical use of biomass.
- **The technical potential** is the usable energy offer with the technical restrictions under consideration of all the other restrictions of the theoretical potential.
- **The economic potential** is the local and temporary part of the theoretical potential that can be accessed under consideration of the given restrictions and its profitability. Economic factors can have temporary influence on the economic potential, for example, the oil price.
- **The exploitable potential** is the usable energy offer from biomass under the restrictions of the potentials above. It is smaller than the economic potential but with time it gets close.

- **The sustainable potential** is the technical potential focused on sustainability requirements. It is restricted by climate and nature protection, but also social austerity has to be considered, for example the food or fuel discussion /2, p.12–14/.

Herbal biomass has forestry, agricultural and aquatic sources. From forestry sources mostly lignocellulosic biomass, like wood and its residues are provided. Agricultural biomass can be lignocellulosic, saccharated, oil containing or starchy, depending on the plant and the parts used from it. Aquatic biomass is mostly micro and macro algae. In this work only lignocellulosic biomass is considered, therefore in the further work the term biomass refers to lignocellulosic biomass.

2.1. Structure of biomass

The main elements of herbal biomass are C, H₂ and O₂. C and O₂ make up around 90 % while the H₂ content is around 6 % /2, p.88/. These elements build the main components of biomass: hemicellulose, cellulose, lignin, starch, sugars and sometimes fats. The other 4 % of the biomass are macro nutrients and trace elements. Important macro nutrients are N₂, K, Mg, Ca, S and P. Trace elements have a concentration lower than 0.03 % of dry biomass and examples are Fe, Cu, Cl₂, Na, Co. Every single element can influence the growth of a plant when its content is too low or too high. Important for this work is the composition of hemicellulose, cellulose and lignin, because they exist in nearly every herbal biomass.

Cellulose is the most common polymer in herbal biomass, with a predominated crystalline structure, a high strength and a high degree of polymerisation, around 10000. It builds the framework of the cell walls and improves the tensile strength of the biomass. The representative formula is (C₆H₁₀O₅)_n and shows that the main component of cellulose is β-1,4-connected glucose, whose structure can be seen in [Figure 2.1](#). Most living beings cannot digest cellulose and it is insoluble in water, which makes biomass with high cellulose content a good alternative to fossil fuel. In wood the cellulose content is between 40 % and 44 %. /2, p.94; 587; 1451–1452/ 3, p.36–37; 74–75/.

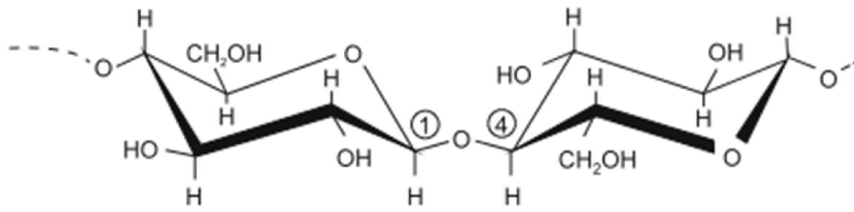


Figure 2.1: Typical structure of cellulose /2, p.588/.

Hemicellulose is a collective term for polysaccharides with a lower degree of polymerisation from 100 to 200. It consists of carbohydrates in a highly branched chain structure with $(C_5H_8O_4)_n$ as its molecular formula. [Figure 2.2](#) shows a xylan structure, which is a common component of hemicellulose. The amorphous structure gives it less strength than cellulose and it gets faster hydrolysed by acids and enzymes. Hemicellulose has many functions in the cell, such as supporting the cell membrane and swelling and sticky effects to stabilise the cell wall. It has more combined moisture than cellulose /2, p.588/ 3, p.37; 80/.

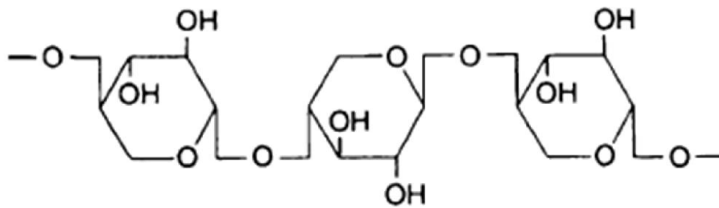


Figure 2.2: Molecular structure of hemicellulose, example: xylan /3, p.37/.

Lignin is a highly branched, three dimensional, aromatic polymer of phenyl propane units, as seen in [Figure 2.3](#). It appears alongside with cellulose and is cementing and hardening the cellulose fibres which allows a plant to stand up. It has the highest C content of these three structures with 64 %, while the O_2 content is around 30 % and H_2 content is around 6 %. Lignin is the second most common component in biomass and it is highly insoluble. Lignin can make up 18 % to 35 % of woody biomass. /2, p. 94; 588–589/ 3, p.38; 81/.

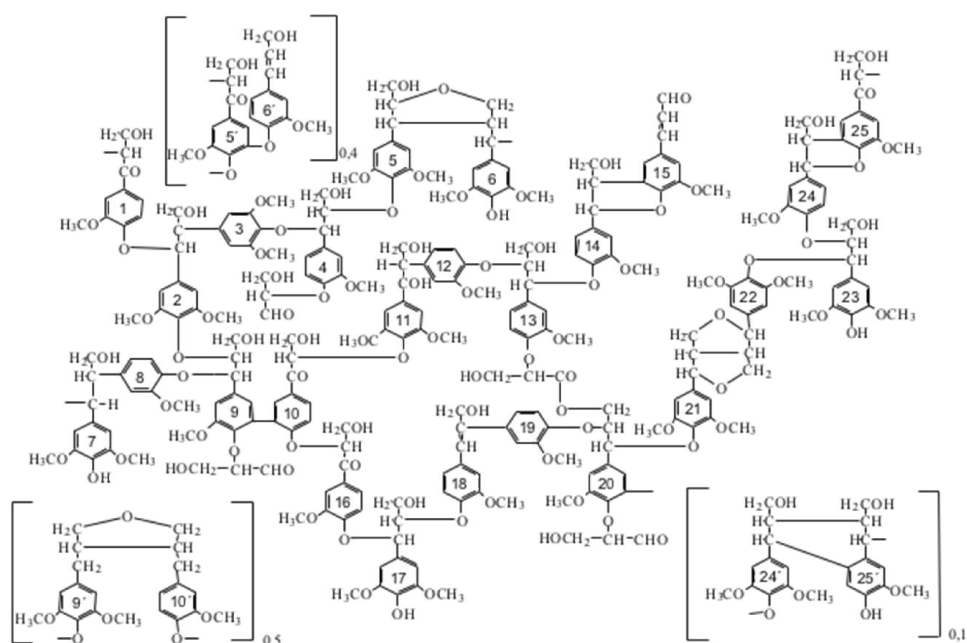


Figure 2.3: Example for lignin structure, beech wood lignin /2, p.589/.

2.2. Biomass as a fuel

Fuel has different physical and chemical properties that define its usage and combustion behaviour. So it is necessary to know these properties of biomass and its products after conversion, to get promising alternatives to conventional fuels. Most important is its higher heating value (HHV) and its chemical composition, because the HHV defines the power the fuel can theoretically accomplish and the chemical composition can give a preview of the products, by-products and wastes of the conversion of biomass, like their degradation behaviour, environmental sustainability, if they are health damaging and of the HHV. Physical properties like bulk density and particle size influence the conversion process of biomass and therefore influence its products, by-products and wastes. It is important to know the base the properties rely on. The four different bases of biomass include different components, as shown in [Figure 2.4](#). The as-received basis (arb) contains all the compounds, including surface moisture, volatile matter and ash, because the material was not processed at all. In the air-dry basis (adb) the sample is dried at open air to remove its surface moisture, the amount of removed surface moisture is calculated by weight difference. To remove the inherent and surface moisture, the sample has to be dried in an oven at 105 °C until the weight is constant. This is called the total-

dry basis (db) and it is the most referred basis. For the dry ash-free basis (daf) the ash content needs to be known to subtract it from the total content. The dry ash-free basis only includes the elemental composition [3, p.56–57]. There are different analyses to determine the components and elements of biomass.

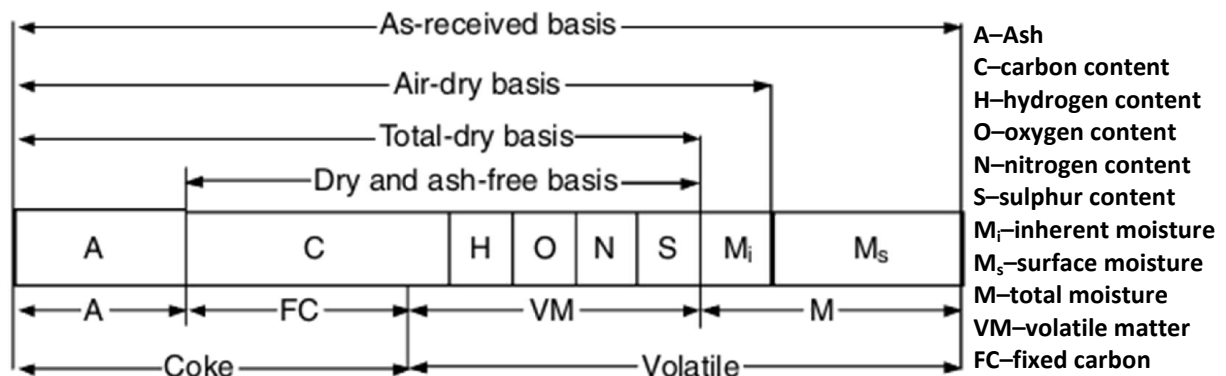


Figure 2.4: Bases of biomass composition [3, p.56/

2.2.1. Proximate analysis

The proximate analysis gives the rough components of biomass like ash (A), fixed carbon (FC), volatile matter (VM) and total moisture. It helps to estimate the products of thermal degradation of biomass. While ash, volatile matter and moisture are determined by standard procedures depending on the raw material, the fixed carbon content is calculated by difference. That is why the fixed carbon does not include the carbon in the volatile matter as seen in [Figure 2.4](#). All contents are given in wt-%. Results of different biomasses can be seen in [Table 2.1](#).

Volatile matter consists of the condensable and non-condensable compounds, which evaporate out of the raw material during the thermal degradation process. Ash is every inorganic solid matter that is left after total combustion of a fuel including potential impurities. The components of ash are mainly macro nutrients and trace elements like Si, Fe and others. Moisture content gives the amount of water contained in the biomass. There are two types of moisture, inherent and surface moisture. Inherent moisture is absorbed inside the cells and is harder to remove than surface moisture that is located outside the cell walls. The fixed carbon content is the amount of solid carbon from the raw material and other carbonaceous residues formed while thermal degradation that are left in the char [3, p.50–54/.

2.2.2. Ultimate analysis

The ultimate analysis gives the elemental composition, the ash and the moisture content of a biomass on a total basis. Typical for an ultimate analysis is the determination of C, H₂, O₂, N₂, and S, other elements can be determined as well, although not all types of biomass even include all of these elements. Moisture and ash content are the same as in the proximate analysis. The results of the elemental composition, the ash and the moisture content are given in wt-%. There are different standard methods for different raw materials. Due to the extra determination of moisture, the H₂ and O₂ content do not include the hydrogen and oxygen that is bound in the moisture. The ultimate analysis is a useful tool to characterise biomass, and its results can be used to predict the HHV (see section [2.2.4](#)), the possible formation of SO_x emissions, the calculation of the oxygen to carbon ratio (O/C), the hydrogen to carbon ratio (H/C) and other estimations /3, p.49–50/. Ultimate analysis results of different biomasses can be seen in [Table 2.1](#).

2.2.3. Thermogravimetric analysis

A different way of analysing biomass is by thermogravimetry (TG) or differential thermogravimetry (DTG). In this procedure a small amount of sample is heated in inert atmosphere, at specified heating rate, in a microbalance. The results give a graph that shows the weight loss over the heating time and delivers results from which moisture and volatile matter can be calculated. To determine the ash content, oxygen has to be introduced in the system. It also delivers information about the degradation process, reaction heat and thermal stability. With this analysis only small amounts of raw material are needed to determine the properties of the fuel /3, p.55–56/.

Table 2.1: Proximate and ultimate analysis results of different biomasses from /4, p.5–6/.

Feedstock	Proximate analysis [wt-%]				Ultimate analysis [wt-%]					HHV [MJ·kg ⁻¹]
	M	VM	FC	Ash	C	H	N	S	O	
Bamboo	9.15	73.92	15.3	1.7– 5.0	45.8 8	5.36	0.32	0.26	37.4	17.82
Corn cob	9.7	80.6	18.2	1.2– 2.8	43.6	5.8	0.7	1.3	48.6	16.9
Hardwood (avg.)	7.8	72.3	25.0	2.7	48.6	6.2	0.4	–	41.1	18.8
Hazelnut shell	9.0	69.3	28.3	4.3	52.3	6.5	5.2	9.2	26.8	19.3
Oil palm fibre*	3.27	71.49	19.1 8	6.06	42.6 5	5.48	1.09	–	50.7 8	15.38
Palm kernel shell	–	77.5	20.3	–	38.9	5.1	0.6	–	32.0	16.3
Rapeseed	8.4	70.0	15.8	5.8	41.1	6.0	5.1	–	47.8	19.4
Rice husk	–	81.6	–	23.5	36.9	5.0	0.4	–	37.9	15.29
Sewer sludge	–	29.01	3.49	67.5	12.7 9	1.74	1.2	0.55	16.2 2	6.56
Softwood (avg.)	8.8	70	28.1	1.7	52.1	6.1	0.2	–	41	20.0
Sugar cane bagasse	8.5	84.0	1.64	4.5– 9.0	45.1 3	6.05	0.3	–	42.7 7	18.17
Wheat straw	8.5	63.0	23.5	5.5– 13.5	53.9	7.0	3.0	–	36.1	17.1
Wood bark	8.8	66.6	31.8	1.6	53.1	6.1	0.2	–	40.6	20.5

* from /1, p. 572 Table 2/

2.2.4. Heating value

There are two heating values for every fuel, the HHV and the lower heating value (LHV). The HHV is the amount of energy that is released during total oxidation of a fuel, including the heat of condensation of the steam. Sometimes it is referred as gross calorific value. The LHV is the amount of released energy without the heat of combustion of the steam, sometimes it is referred as net calorific value. Biological fuels have a difference between the HHV and the LHV of 6 % to 7.5 % referred to absolute dry biomass. When the biomass contains water, the difference gets higher /2, p.607–608/ 3, p.58/. When the HHV of the dry biomass is known by measurement, the LHV of as-received biomass can be estimated by the following equation:

$$\text{LHV} = \text{HHV} \cdot \left(1 - \frac{M}{100}\right) - 2.447 \cdot \frac{M}{100} - \frac{H}{100 \cdot 2} \cdot 18.02 \cdot 2.447 \cdot \left(1 - \frac{M}{100}\right) \quad (2-1)$$

With: LHV – lower heating value [$\text{MJ} \cdot \text{kg}^{-1}$]

HHV – higher heating value [$\text{MJ} \cdot \text{kg}^{-1}$]

M – moisture content [wt-%]

H – hydrogen content [w-%] /5, p. 19/

In this work only the HHV is used, therefore the LHV gets no further observation.

For the estimation of the HHV different equations can be used, some are general for fuels; others depend on the aggregate state. The most common way is to estimate the HHV from the results of the ultimate analysis of the fuel.

Two equations are given here as examples for general estimations of the HHV of fuels. Equations for char and bio-oil are found in section 3.1.

The first equation is for dry and only solid biomass:

$$\text{HHV} = 1.87C^2 - 144C - 2820H + 63.8C \cdot H + 129N + 20147 \quad (2-2)$$

With: HHV [$\text{kJ} \cdot \text{kg}^{-1}$]

C – carbon content [wt-%]

N – nitrogen content [wt-%]

Relative error is 4 % /2, p.611/

Another correlation is for dry biomass, gas, liquid and coal:

$$\text{HHV} = 349.1C + 1178.3H + 100.5S - 103.4O - 15.1N - 21.1A \quad (2-3)$$

With: HHV [$\text{kJ} \cdot \text{kg}^{-1}$]

S – sulphur content [wt-%]

O – oxygen content [wt-%]

A – ash content [wt-%]

The validity ranges of this correlation are:

- $0 < C < 92.25 \%$; $0.43 < H < 25.15 \%$; $0 < O < 50 \%$; $0 < N < 5.6 \%$; $0 < \text{Ash} < 71.4 \%$;
 $0 < S < 94.08 \%$
- $4.7447 < \text{HHV} < 55.345 \text{ kJ} \cdot \text{kg}^{-1}$
- The absolute error is 1.45 % /6, p.1058/

The HHV can be expressed on the different bases, but for a better comparison it is more common to relate the HHV on a dry basis. Examples of HHVs for different types of biomass are given in [Table 2.1](#).

The O/C and the H/C ratios influence the HHV and the character of a fuel as well. The van-Krevelen-Diagram ([Figure 2.5](#)) displays a comparison of different fuels according to their H/C and O/C ratios. It shows that an increasing H/C ratio and a decreasing O/C ratio increase the HHV of fuels. In the degradation of biomass these ratios are only important in the char, generally the degradation process leads to smaller H/C and O/C ratios in chars than in the raw material [/7, p.2272/](#). Higher ash and moisture content lower the HHV and LHV as well, as seen in [Figure 2.6](#).

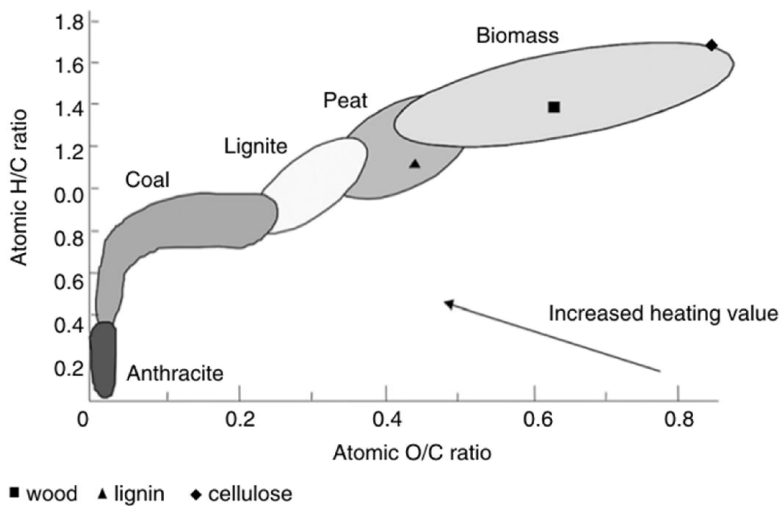


Figure 2.5: Van-Krevelen-Diagramm, Atomic ratios of different fuels [/3, p.39/](#).

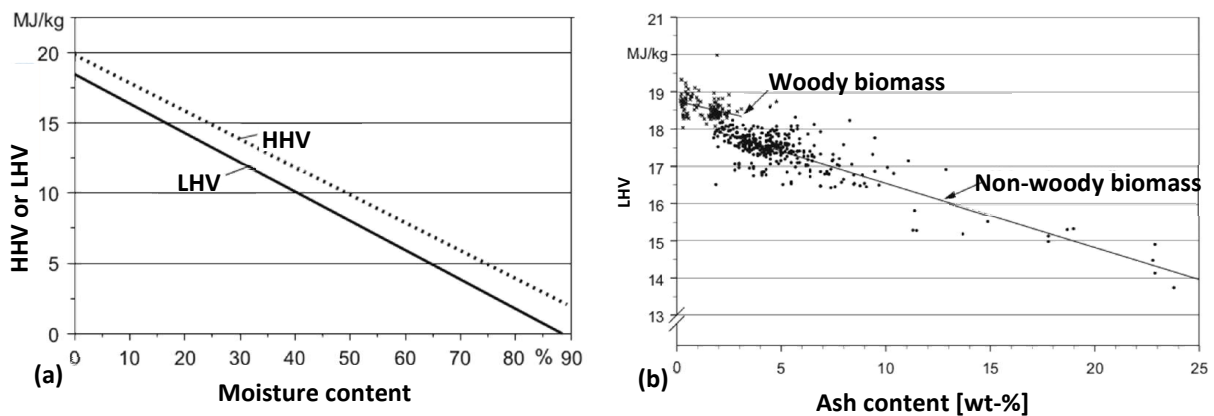


Figure 2.6: (a) Influence of moisture content on the HHV and LHV [/7, p.610/](#)
 (b) Influence of ash content on LHV [/7, p.612/](#).

2.2.5. Other properties

There are many other properties that can characterise a fuel. Biomass, for example, has physical, chemical and thermal properties that affect its behaviour before and during its transformation to useable energy. Form, size and particle size distribution of the biomass are necessary to know, for example, if a mechanical treatment of biomass is needed before its combustion. They have influence on the ignition, degradation and drying behaviour, but also on other process parameters like the bulk density. These properties need to be matched to the reactor system with all possible pre- and downstream-processing. The bulk density is another important attribute of biomass; it is defined as the total mass of a defined amount of biomass particles divided by the space they occupy. Therefore it includes the space between the biomass particles and it is important to know for the storability and the transportability of the biomass. It is connected to the energy density. Pelletising can raise the bulk density and increase the energy density. For pelletised biomass the abrasion resistance can give information about transportability and dust formation /2, p. 620–625; 629; 636/ 3, p.43/.

Macro nutrients and trace elements have different influences too. Besides C, higher K, Mg, Na, Ca and other contents lead to higher emission of particles. High temperature corrosion can occur with high K, S and Cl₂ concentrations. S and N₂ can lead to dangerous SO_x, NO₂ and NO_x emissions, while heavy metals increase the risk of heavy metal emissions. This is just a gross overview of properties that need to be considered while processing biomass /2, p.580–581 Table 11.1/.

3. BASICS OF PYROLYSIS

Biomass can be processed in mainly three ways: thermo-chemical, physico-chemical and biochemical [2, p.6]. Pyrolysis belongs to the first group, the thermo-chemical conversion. Alongside with it, there are torrefaction, gasification and hydrothermal transformation.

In the action of thermo-chemical conversion, heat and sometimes catalysts, are used to transform mostly solid biomass, as a primary energy carrier, into secondary energy carriers of any aggregate state with a higher energy density.

In the physico-chemical conversion mostly biomasses with high oil content are processed by separating the oil phase from the solid phase, for example, by mechanical squeezing.

The biochemical processes use microorganisms to decompose the biomass into secondary energy carriers or useful energy.

Pyrolysis uses external heat to decompose long hydrocarbon chains, which are the main components of biomass, to smaller molecules while oxygen is absent. The products are liquid oils or tar, solid char and non-condensable gases, whose yields vary with different pyrolysis conditions and reactor types. The yield of a product phase is the ratio between the remaining mass of any aggregate state divided by the mass of the sample before pyrolysis.

$$Y_i = \frac{m_i}{m_s} \cdot 100 \% \quad (3-1)$$

With: Y_i – yield of solid, liquid or gas [%]

m_i – remaining mass of solid, liquid or gas [g]

m_s – sample mass [g]

The main parameters that influence the pyrolysis process and its products are the temperature, the heating rate and the gas residence time.

3.1. Influence of temperature on the pyrolysis performance

In the pyrolysis processes the temperature has a moderate range of 300 °C to 900 °C compared to other thermo-chemical conversion processes. According to its actual temperature pyrolysis can be differentiated into four stages. The first stage is the

drying of the sample up to around 100 °C. In this stage the uncombined moisture evaporates from the biomass which gives better heat transfer to the interior of the biomass particles. After drying, the next stage occurs from 100 °C to 300 °C. This stage initiates the heating of the biomass, while water and molecular-low-weight-gases are released. Followed by the second stage is the intermediate stage, with a temperature range of 200 °C to 600 °C, which can also be referred as the primary pyrolysis. In this stage the main reactions take place, the products are released as vapours with non-condensable and condensable compounds; also large hydrocarbon molecules are broken down into char. The final stage proceeds from around 300 °C until 900 °C, the high temperatures lead to a secondary cracking of the volatile compounds into secondary char and non-condensable gases. This stage can also be called secondary pyrolysis. As the temperature ranges show, these processes do not happen strictly one after another, but overlap in their ranges. This is due to the inhomogeneous properties of most biomass types, for example, particle size and form; this makes an even heating of the biomass nearly impossible /3, p.65; 77–78/.

The temperature has not only an influence on the product yields, but also on its compositions. The main compound of the char is C and some ash, but it can also contain chemically bonded O₂ and H₂. Increasing temperature leads to a decreasing char yield because of the on-going release and cracking of volatiles /3, p.70; 75/ 8, p.581/ 9, p.170/. H₂ is released as molecular hydrogen and O₂ can be released as CO, CO₂ or molecular-low-weight-hydrocarbons /2, p.1233/.

A higher temperature leads to a higher fixed carbon content of the char in different types of biomass. This is also due the on-going cracking and releasing of volatiles /8, p.583/ 9, p.170/. The yield of the liquid phase, in general, has a maximum between 400 °C and 500 °C /2, p.659/ 8, p.581/ 9, p.169, Table 2/. The optimum is in this range because the volatiles escape from the sample, but the temperature is not high enough for the secondary cracking to occur. Compounds of the liquid phase are mostly hydroxylaldehydes, hydroxylketones, furans, sugars, carboxylic acids, alcohols, phenolic compounds and water, depending on the raw material and experimental conditions /1, p.573/ 3, p.70/ 8, p.584/ 9, p.171/ 10, p.1328/ 11, p.79/. Because of

the secondary pyrolysis, the gas yield increases with increasing temperature. Most of the experiments done so far, show that the main components of the gas phase are CO, CO₂, H₂ and hydrocarbons, such as CH₄, C₂H₆ and C₂H₄ /1, p.576/ 3, p.70/ 9, p.174 Table 4/ 10, p.1325/ 11, p.79/ 12, p.619/. The H₂ content of the gas phase usually increases with increasing temperature, the CO₂ content decreases as the temperature gets higher, CO also decreases, but it reaches a stable low level around 600 °C. The hydrocarbons have a maximum release between 400 °C and 600 °C, but this peak depends on the raw material /3, p.76 Figure 3.6/ 9, p.174 Table 4/ 10, p.1325/.

Due to its influence on the chemical composition of the pyrolysis products, the temperature has an influence on their HHVs as well. The HHV of the char, in general, increases until around 600 °C, but at higher temperatures it remains nearly constant, with a slight decrease /8, p.583 Table 4/ 9, p.169 Table 2/. The HHV of the char can be predicted by the following equation:

$$\text{HHV}=0.2949\text{C}+0.825\text{H} \quad (3-2)$$

With: HHV [MJ·kg⁻¹]

C;H [wt-%]

The relative error is below 15 % /1, p.575/.

In the liquid phase, the HHV is not only decisively influenced by the temperature. Only /9, p.171/ mentions a decrease in the HHV for temperatures above 600 °C, because of the secondary cracking. The work by Chen and Lings shows a maximum value for the HHV of the liquid phase at 450 °C, but only a temperature range from 400 °C to 500 °C was investigated /1, p.575 Table 3/. In this work there is an equation given for the proximate HHV of bio-oils:

$$\text{HHV}=0.3382\text{C}+1.4428(\text{H}-0.125) \quad (3-3)$$

With: HHV [MJ·kg⁻¹]

C;H [wt-%]

The relative error gets high till 29.1 %, this is due to water in the oil, the equation should only be used for water-free bio-oils /1, p.575/.

As the H₂ content is proportional to the HHV, the HHV of gases increases with higher temperatures /7, p.2272/ 9, p.174/ 13, p.594 Table 4/.

3.2. Influence of heating rate and gas residence time on the pyrolysis performance

According to the heating rate (HR), pyrolysis can be differentiated into fast and slow pyrolysis, with flash pyrolysis being a special type of fast pyrolysis and torrefaction being a special type of slow pyrolysis. In fast pyrolysis the heating time is lower than the reaction time and in slow pyrolysis the heating time is much higher /3, p.71/. The gas residence time is another factor that influences the products, the shorter it is, the less secondary cracking happens, which leads to higher liquid yields. Depending on the favoured product, there are three main operating conditions for the pyrolysis:

- For char maximisation a low heating rate, a low final temperature and a long gas residence time are required;
- The operating conditions for the maximum liquid yield are a high heating rate, medium final temperatures and a short gas residence time;
- For a maximum gas yield, the references go along with each other for a high final temperature and a long residence time, but for the heating rate, the two references /2/and /3/ have some difference. One gives a high heating rate for the maximum gas yield /2, p.659/ the other one a slow heating rate /3, p.77/.

The difference in the heating rate specification for the gas yield does not seem to be a decisive factor, because the long residence time and the high final temperatures lead to secondary cracking from volatiles into non-volatiles, which leads to a higher gas yield.

3.2.1. Fast pyrolysis

In fast pyrolysis the main goal is to speed up heat and mass transfer in order to maximize the yield of the liquid phase. To attain this, high heating rates from 1000 °C·s⁻¹ until 10000 °C·s⁻¹, a short gas residence time, below 2 s, reaction temperatures up to a maximum of 650 °C and fast cooling of the vapours are needed. The short gas retention time and the maximum temperature of 650 °C prevent secondary cracking into non-volatile gases. If the gas retention time is higher, there

could be secondary cracking when the vapours get in contact with the hot char, which can work as a catalyst. Higher temperatures lead to secondary cracking too, as described in the previous section. Another effect of the secondary cracking is that it promotes a phase separation in the liquid phase in an aqueous and a tarry fraction.

Fast pyrolysis has three steps. At first there is the physical pre-processing of the biomass, for example drying, mechanical grinding, separation etc. Afterwards follows the pyrolysis itself, with rapid cooling of the volatiles, and the last step is the downstream-processing. In the downstream-processing the products, mainly the oil, get refined by chemical or physical treatment to get the requested properties for the requested application. With the right conditions for the raw material, the liquid yield of fast pyrolysis can go up to 75 %.

In flash pyrolysis the gas retention time is even shorter, from 350 ms to 1500 ms, while the final temperature stays the same and the heating rate is near the end of the range of the heating rates of fast pyrolysis /2, p.1197–1198/ 3, p.73/.

3.2.2. Slow pyrolysis

Slow pyrolysis methods, for example, carbonization are used for a long time to fabricate coal from wood. Because optimization of the solid product is in the spotlight in this process, the temperature is mostly limited to a maximum of 600 °C. There is no specified heating rate of slow pyrolysis, but is in the range of degrees celsius per minute. Also, the gas retention time is in the range of minutes if char is the main product to be obtained. The solid yield can reach up to 30 % /2, p.1223/ 3, p.72/.

Torrefaction is a special form of slow pyrolysis, working with temperatures between 200 °C and 300 °C, a low heating rate below 50 °C·min⁻¹ and a residence time in the range of minutes. The aim is to improve the fuel properties of raw biomass for further conversion. Water and volatiles are released; these components come mainly from the depolymerisation of hemicellulose, which occurs in this low temperature range (see section [3.3.1.](#)). Lignin and cellulose decomposition starts in this temperature range, but it finishes at higher temperatures (see section [3.3.1.](#)). The increased properties of torrefied biomass when compared to raw biomass are:

- Higher HHV through the reduction of the moisture and CO₂ content;
- Better grinding ability through higher brittleness;
- Higher energy density through higher relative C and H content;
- Less moisture absorbance through hydrophobising, because no H₂ bonds are formed;
- No biological activities which could lead to biological degradation;
- Weight loss and better handling.

Although the HHV of torrefied biomass is higher than the HHV of raw biomass, the energy density decreases due to the lower bulk density after torrefaction /2, p.1236–1238/ 3, p.92–94/.

3.3. Other parameters that influence the pyrolysis performance

Apart from the three discussed parameters discussed before, there are other process parameters and biomass characteristics that can influence the outcome of the pyrolysis products, such as chemical and physical properties of the raw material and flow rate of the inert medium.

3.3.1. Chemical composition of the raw material

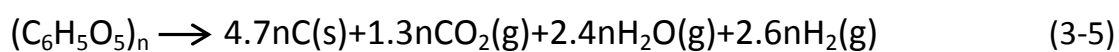
The contents of cellulose, hemicellulose and lignin have a big influence on the pyrolysis process and its products; because of the different degradation reactions they yield different components at various temperatures.

According to the modified Broido-Shafizadeh model the complex degradation of cellulose is separated into three main steps. The first step is a pre-reaction that forms active cellulose at temperatures from 150 °C to 220 °C. In this process the bonds between the glucose molecules are broken down and the degree of polymerisation decreases. This isomerisation reaction is simplified to:



(-1.5 < ΔH < 0 kJ·equiv.mol⁻¹) /2, p.662/ 14, p.1162–1163/

Degradation steps two and three do not follow each other. They are competing first order reactions. The second step includes dehydration, decarboxylation and carbonisation. The carbonisation reaction is given by the following equation:



$$(\Delta H = -170.17 \pm 7.27 \text{ kJ} \cdot \text{equiv} \cdot \text{mol}^{-1}) \quad /14, \text{ p.1162–1163/}$$

While carbonisation is favoured at low heating rates and temperatures below 400 °C, decarboxylation can also happen at higher temperatures /2, p.663/ 3, p.79/ 14, p.1162–1163/. The whole process of carbonisation is exothermic and Figure 3.1 shows that normally exothermic degradation processes happen at higher temperatures, but this does not compare with /3, p.79/ 14, p.1165/. This reaction path mainly produces char, CO, CO₂ and H₂O vapour. At higher heating rates and temperatures the dehydration and decarboxylation can form ethanoic acid, formic acid and ethylene glycol /2, p.663/. Probably the exothermic carbonisation takes place at lower temperatures, while decarboxylation, which happens also at a higher temperature range, might be endothermic and consumes more heat than the carbonisation delivers, so the whole process stays endothermic /15, p.1784/. At this point the modified Broido-Shafizadeh-Model might not be accurate. In the third step the depolymerisation and scission happen at lower temperatures and heating rates /2, p.663/. A simple equation for this reaction is given in the following equation:



$$(\Delta H = 131.38 \pm 2.42 \text{ kJ} \cdot \text{equiv} \cdot \text{mol}^{-1}) \quad /14, \text{ p.1162–1163/}$$

The products are glycosans, like levoglucosan, that when slivering water can produce tars. This process is endothermic which means that it is favoured by lower temperatures /2, p.662–663/ 14, p.1163 Table 1; 1165/ 15, p.1784 Figure 3/ contrary to /3, p.79/. The whole process of its degradation is endothermic till 400 °C and then goes exothermic. There is a big endothermic peak around 350–380 °C as seen in Figure 3.1. After all, the decomposition of cellulose leads to form oxygenates, furans and sugars, but compared to hemicellulose it yields more condensable vapours and therefore it is the main contributor for bio-oil. In the gaseous phase the decomposition of cellulose only releases a small amount of the CO content and in the

solid phase it only contributes with small amounts /1, p.573; 576/ 3, p.74–75/ 15, p.1783–1784/. The degradation temperatures of the three components vary in every reference, for cellulose the temperature range is from 275 °C to 350 °C /3, p.74/ (315–400 °C /1, p.572/; 300–400 °C /8, p.581/ or 250–360 °C /9, p.174/).

The breakdown of hemicellulose is similar to the one of cellulose; it is an endothermic process until around 200 °C and gets exothermic until 500 °C. The main decomposition of hemicellulose is done even before the one of cellulose, but after 500 °C the process turns endothermic again as seen in [Figure 3.1](#). A higher hemicellulose content leads to a higher non-condensable gas and a lower liquid yield /2, p.588; 1452/ 3, p.37–38/. The decomposition and the cracking of hemicellulose release CO and CO₂ in the gaseous phase, because these gases are formed at lower temperatures. Like cellulose it leads to the formation of oxygenates, furans and sugars, which again form esters, acids, alcohols, ketones and aldehydes in the liquid phase, but it gives a higher contribution to the char yield /1, p.573; 576/ 15, p.1783–1784/. The temperature range of the degradation of hemicellulose is from 150 to 350 °C /3, p.74/ (200–315 °C /1, p.572/; 200–300 °C /8, p.581/ or 220–320 °C /9, p.174/). Hemicellulose and cellulose can be summarised under the term of holocellulose. Biomass with a high holocellulose content produces more volatiles /7, p.2273/ 11 p.82/.

Lignin degradation starts with the release of water and CO₂ at low temperatures. At higher temperatures up to 400 °C, it releases phenolic compounds, CO₂, water and CH₂O (formaldehyde). When the temperature reaches 600 °C, it mainly releases CO, CO₂, CH₄, H₂ and CH₃OH (methanol). The CO and CO₂ amounts in the gas phase are minor at lower temperatures and the amounts of CH₄ and H₂ are the highest from all components/2, p.663/ 15, p.1787/. In the liquid phase it produces mainly phenolic compounds /3, p.81/. Due to the high C content of lignin, around 64 %, it yields most of its weight to the solid phase as char when decomposed. The char composition varies with temperature, at low temperatures there are still OH groups in the aromatic compounds, around 600 °C it is mainly aromatic char /2, p.663/. In general a higher lignin content leads to a lower release of volatiles /1, p.567; 573/ 11, p.82/ 12,

p.2270; 2273/. Figure 3.1 shows that this process is endothermic until 180 °C and when the main pyrolysis starts, it is exothermic again until the end. The degradation temperature range of lignin is from 250–500 °C /3, p.74/ (160–900 °C /1, p.572/; 200–900 °C /8, p.581/ or 180–500 °C /9, p.174/).

With a higher ash content there is a higher possibility of cracking, due to ash working as a catalyst, this can lead to decrease in the liquid yield and also to its separation into an aqueous and a tarry phase /2, p.1197/ 13, p.592/.

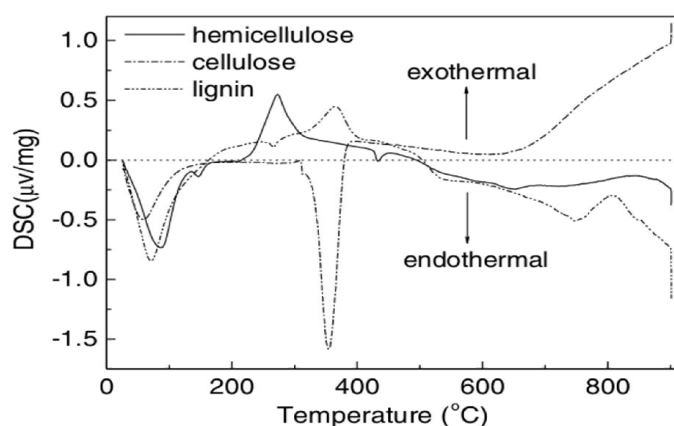


Figure 3.1: DSC curves of hemicellulose, cellulose and lignin pyrolysis /15, p.1784/.

3.3.2. Carrier gas flow rate

In most of the laboratory scale pyrolysis experiments the carrier gas used is N₂. Only a few studies are made with a different inert atmosphere, for example, H₂ or a vacuum. This is due to the low cost of N₂ for the small amounts used in laboratory scale, but in industrial pyrolysis there is most of the time no carrier gas at all. When an industrial scale pyrolysis starts, the oxygen in the leftover air reacts in the beginning and when it is depleted the reaction atmosphere is rendered inert. The flow rate of the carrier gas has an influence on the gas retention time; the influence of the gas retention time is described in section 3.2. A higher carrier gas flow rate can lead to the dilution of the gaseous product in the carrier gas and it can also prevent the total condensation of the condensable compounds when they are carried too fast through the condensers, this leads to a lower liquid yield. On the other hand, if the flow rate is too low it can promote secondary cracking of the volatiles, which leads to a lower liquid yield too /7, p.2266/ 16, p.189–191/. A low carrier gas flow rate can promote

an increase in the char yield. The carrier gas flow rate should be adjusted to the requested outcomes.

3.3.3. Physical properties of the raw material

The particle size of the feed can have a major influence on the pyrolysis conditions. With larger particles, there is a higher chance of temperature gradients inside the particle. With a temperature gradient inside a bigger particle, different reactions can take place in different zones of the same particle. While the outside is hotter and already undergoes the degradation, including the release of moisture and volatiles, the intermediate part might just start the degradation process, while the inner part of the particle could still be in the drying process. Therefore, bigger particles do not have a uniform heating rate and limit the degradation process through heat and mass transfer. The mass-transport-limitation occurs more dominant at higher heating rates /7, p.2266/ 12, p.613–614/. Samples with smaller particles have a higher bulk density and therefore the carrier gas cannot flow through as easily, which leads to an increasing retention time of the gaseous phase and this can promote secondary cracking. On the other hand, smaller particles release volatiles more easily, so they can be carried out before they undergo secondary cracking /3, p.75/. The flow rate and particle size have to be geared to each other. With particle sizes below 2 mm the liquid yield increases with the particle size, while the gas yield decreases and the solid yield stays nearly constant. Particle sizes above 2 mm show the opposite trend on the pyrolysis yields: the liquid yield decreases slightly with an increase in particle size, while the gas yield increases /7, p.2265–2266/ 17, p.248–249/.

3.4. Types of pyrolysis reactors

This section gives an overview of the types of reactors that are used in pyrolysis. The different reactor types are built for different purposes, depending on the requested product. Typical yields are always given in relation to the total-dry raw material. Pyrolysis reactors that are described in the following sections can be seen in Figure 3.2.

3.4.1. Fixed bed reactors

Fixed bed reactors are the oldest type of reactors. They have been in used for ages to produce coal from wood. A fixed bed reactor is made of a container that contains a stationary bulk of one or more reactants. Most of the time a fluid is flowing through the fixed bed and in pyrolysis processes it is mostly used to produce a high solid yield. To improve the solid yield, the raw material should be dried before. These kinds of reactors are mostly used in slow pyrolysis processes (see section [3.2.2.](#)).

- **Kilns:** One simple form is called charcoal kiln or beehive oven. The easy design is made of soil, stonework or metal. In these reactors a pile of wood is placed inside and the heat is created from a small fireplace that is also located inside the reactor. Therefore a small hole has to be in the wall to provide the oxygen supply for the fire. Due to the fire, the raw material undergoes a partial combustion. The produced gases escape through holes on top of the kiln. Depending on the construction of the kiln, the moisture of the raw material and the skills of the operator, the char yield can be between 20 % and 25 %. On the one hand, kilns have a cheap design and easy handling and operating conditions, but on the other hand, it exposes operators and environment to the untreated pyrolysis gases that are released. This process can take more than 10 days to be completed. This still the main procedure for the making of coal from wood /2, p.1223–1226/.

In more modern reactor types, the heat is provided either through external heating or an internal heated carrier medium.

- **Reactors with external heating:** These reactors provide the necessary heat through the reactor wall, while the raw material is placed inside. The heat is mostly provided by the combustion of the produced gases. In the beginning, where non-flammable gases emerge, the process needs to be heated by other sources, for example, electricity or fossil fuels. Gas escapes the reactor because of volume expansion or is carried out by a carrier gas. Intermittent mode of operation has nearly no importance to the industry, but in laboratory scale pyrolysis it is still in use. A continuous mode of operation is also not

common in the industry because of the elaborate design. After the initial stage, the process can heat itself by combustion of the produced gases. In this kind of modern reactors the char yield can be up to 30 % because the raw material does not undergo a partly combustion in the beginning. As all the volatiles get burned in this process, the liquid yield should be minimalized /2, p. 1226–1228/ 3, p.87/.

- **Reactors with internal heating:** The heat is provided by a hot gas flowing through the reactor. This can be a pre-heated inert gas or the gas produced by the pyrolysis. In the quasi-continuous Reichert process several reactors are operated simultaneously. The heat is provided by an inert gas that is heated through the combustion of the pyrolysis gas. The volatiles flow through condensers, and afterwards there is a separation between the carrier gas and the condensable components. Therefore this process leaves some liquids. When wood is the raw material these liquids are used to produce acetic acid and smoke gas flavours /2, p.1228–1229/.

3.4.2. Moving bed reactors

Moving bed reactors are more common in industrial use. There is a wide range of reactor types depending on the raw material and the preferred products. Most of them are used to produce a useful liquid phase and are operated on the conditions of an optimal liquid yield. Some special types are used for the optimisation of the solid yield. Reactors with moving beds are used for fast pyrolysis; a consistent heat transport and an effective mass transfer are provided by a hot solid, mostly sand, or gas that is mixed with the raw material through pneumatic or mechanical power input. To be fluidised the raw material needs to have small particle diameters (d_p) /2, p.1199/.

3.4.2.1. Reactors with pneumatic power input

- **Bubbling fluidised bed reactor:** Their simple design includes a bubbling bed of inert solids that is heated either internally or externally; in this preheated bed the biomass degradation takes place. The gaseous phase is normally collected on the top of the reactor and it is cleaned from solid sand and char particles in

a following cyclone. Afterwards it is cooled down rapidly in a quench and the emerged liquid is stored. To improve the liquid yield and to get out the fine droplets of the aerosol, the cooled gas can be further processed in electrostatic precipitators. For the fluidisation of the bubbling bed, an inert gas or the produced and cleaned pyrolysis gas are used. The char and a part of the non-condensable gases can be used for the heating of the process. It is important to separate the chars from the produced vapours, for example by elutriation because they can have catalytic influence on the secondary cracking which can lead to a lower liquid yield (see section 3.1.). The solids have a much higher retention time than the gases. Through the intense mixing of solid particles and biomass, this process offers good and steady temperature control, heat transfer and it is also easy to scale up. The liquid yield is around 70–75 % /2, p.1199–1203/ 3, p.87/.

- **Circulating fluidised bed reactor:** These reactors work in a similar way as the bubbling bed ones. The difference is that the reactors have a fully fluidised bed and the solids are continuously recycled. With this kind of bed, the reactor achieves very high and uniform heating rates, short residence times and a very accurate temperature control. Higher flow rates of the hot carrier gas are needed which lead to higher abrasion of the char and more fine particles in the gaseous phase. The solid phase has a similar or even shorter residence time than the gas. Like in bubbling bed reactors, the inert solids and char get out at the top of the reactor with the vapour and are separated in following the cyclones. After the separation from the solids, the vapour is condensed rapidly in a quench and the liquid is stored. The separated sand returns to the reactor bed and the separated char is combusted with the non-condensable gases to provide the heat for the process. This process is running in industrial scale in Canada, called rapid thermal pyrolysis (RTP) and in Finland. The liquid yield can go up to 83 % /2, p.1203–1205/ 3, p.88/.
- **Ultra-rapid pyrolyser:** The reactor is heated internally either through a preheated carrier gas or a heat carrying solid, that is heated to 100 °C above

the set point of the reactor. A very high velocity of the carrier gas is needed to provide extremely short mixing, residence and quenching times. The biomass is fed on top of the reactor together with the carrier gas or solid inlet. While they fall, they mix and the biomass is heated in milliseconds. On the bottom of the reactor the product gets cooled rapidly. The liquid yield can be increased to 90 % /3. p.88/.

- **Fluidised bed reactor for char production:** A special type of fluidised bed reactors can be used for the production of char. This type of reactor has no inert solid material, so there is no circulation. The raw material needs to have small and uniform particle size and is injected to the preheated inert gas flow on the bottom of the reactor. Because of the degradation the char has a lower density than the raw material and is discharged with the gas on top and has to be separated in a cyclone. The main problem is the mixing of the pyrolysis gas with the carrier gas which decreases the HHV of the produced gas constantly. Therefore the gas combustion is more difficult, which leads to problems in the providing of the heat. This kind of reactors are not in industrial use yet /2, p.1231/.

3.4.2.2. Reactors with mechanical power input

- **Rotating cone pyrolyser:** The engine powered rotating vertical cone is placed inside a stationary container. Preheated sand and biomass are fed to the bottom of the rotating cone and get mixed with each other. Through centrifugal force the mixture is pushed to the hot inside wall of the cone and crawls up slowly. On its way to the top of the cone the pyrolytic conversion happens. When the solid mixture reaches the top it falls down into the stationary container, where the char either is burned in a fluidised bed to heat the cone and the recycling sand or it is separated from the sand and combusted to provide heat indirectly. The gaseous phase is removed and cooled quickly and the non-condensable gases can be used for the heating or other thermal applications. The fast cone rotation of 360–960 min⁻¹ supports short solid residence times around half a second. A big advantage of this

reactor is that there is no need for an inert gas. The typical liquid yield is between 60–70 % /2, p.1205–1206/ 3, p.89/.

- **Twin screw reactor:** In this reactor type the inert solid is quasi-fluidised by a twin screw. Through mechanical fluidisation the heat loss is minimised compared to the one in a fluidized bed with a hot carrier gas. The biomass mixes with the hot sand in the vertical twin screw and is degraded in seconds. Gas and small char particles get out on top of the reactor and are separated in cyclones. After the separation, the gas is condensed and the remaining liquids in the aerosol are separated in an electrostatic precipitator. While the liquid is stored, the non-condensable fraction of the gas can be used to heat the recycling sand. The output for the rest of the char is on the bottom of the reactor. This char can also be burned for the heating of the process. Sometimes this process is used to produce pyrolysis slurries that can be easily utilised for the production of syngas. The particle size distribution of the char particles is decisive for a transportable and storable mixture. The liquid yield is between 40 % and 70 % and the solid yield is 15–40 % /2, p.1206–1207/.
- **Ablative pyrolyser:** In ablative reactors the biomass is degraded by the direct contact with a hot surface. This provides excellent heat transfer. The raw material melts and leaves a liquid residue that evaporates immediately. This effect can be enhanced by a moving hot surface and an intense pressing of the biomass against the wall. The pressing force is either created by mechanical or centrifugal force. There is no need for a carrier gas because the pyrolysis gases escape quickly through their volume expansion. Like in most of the other reactors, the gas flow is condensed and the liquid is stored. The advantage of working with this type of reactor is that the particle size does not impair the process quality, but through its elaborate design and geometry it is hard to scale up. Ablative pyrolysers can be built as cyclones, centrifugal reactors or reactors with a rotating surface like plates or barrels. The liquid yield is up to 80 % /2, p.1208–1210/ 3, p.89/.

- **Vacuum pyrolyser:** The biomass is inserted in a vacuum chamber where it is heated on the surface of a moving conveyer band or moving plates. The movement guaranties that the raw material is turned over and moved through the reaction zone. Because of the vacuum no inert solid or carrier gas is needed and the produced gases are removed very quickly by the vacuum pump. The vapours are treated in a similar way as in the other processes and the non-condensable gases can be used for the heating by combustion. Retention times of the biomass are up to 30 minutes and the liquid yield is 35–50 %, while the char yield is relatively high too /2, p.1210/ 3, p.89/.

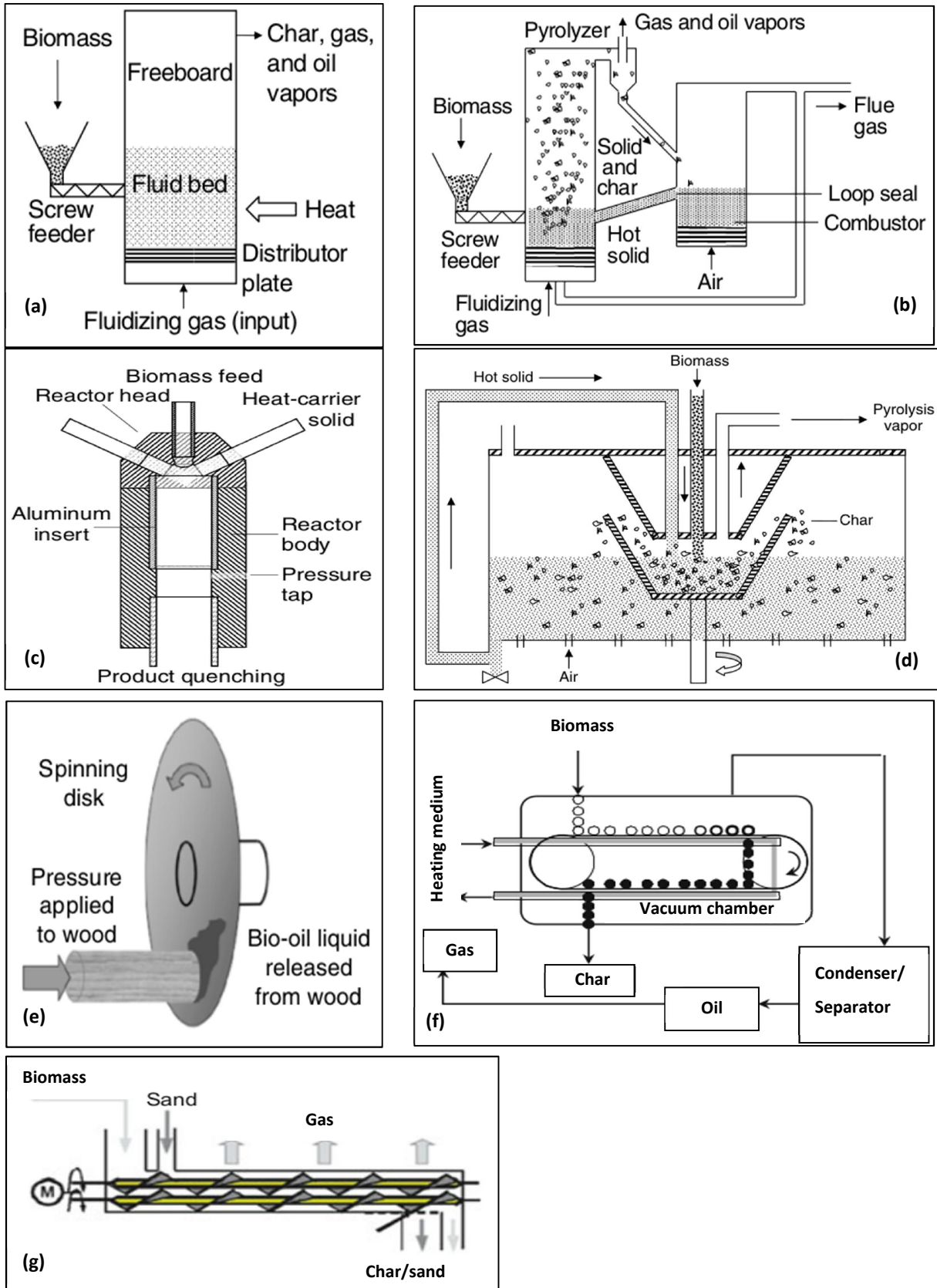


Figure 3.2: Different reactor types: (a) Bubbling bed; (b) Circulating fluidised bed; (c) Ultra-rapid; (d) Rotating cone; (e) Ablative /3, p.86/; (f) Vacuum; (g) Twin screw /7, p.1200/.

4. PYROLYSIS OF OIL PALM RESIDUES

4.1. Introduction

For every tonne of palm oil produced there are 990 kg of usable biomass that is composed of 220 kg of empty fruit bunches (EFB), 670 kg of OPF, 70 kg of oil palm shell (OPS) and 30 kg of palm kernel cake (PKC) /8, p.577/. Indonesia and Malaysia are the main regions where oil palms are cultivated, followed by Africa, where the plant has its origins, and South America. In the two countries the palm oil industry is a main provider of jobs and they produce around 85 % of the world's palm oil and export around 90 % of it /18, p.2407; 2414/. The demand of palm oil, although it already has the highest percentage of the vegetable oil use worldwide (33 %), is still increasing because of its many applications and low price. The oil from the fruits is used in foodstuff industry, while the oil from the kernel is used in cosmetics industry and can be processed to bio-diesel which makes up the 5 % of economical diesel. Oil palms are useful because with $3.74 \text{ t}\cdot(\text{ha}\cdot\text{year})^{-1}$ they have by far the highest oil yield per hectare of all oils plants, also a high oxygen release ($21.3 \text{ t}\cdot\text{ha}^{-1}$) and CO_2 absorbance ($29.3 \text{ t}\cdot\text{ha}^{-1}$) in comparison to soybean with an oil yield of only $0.38 \text{ t}\cdot(\text{ha}\cdot\text{year})^{-1}$, an oxygen release of $2.56 \text{ t}\cdot\text{ha}^{-1}$ and a CO_2 absorbance of $3.52 \text{ t}\cdot(\text{ha}\cdot\text{year})^{-1}$ /18, p.2407 Table 1; 2414/. Due to its high demand the downstream-processing of oil palm industry is becoming an industry itself where the biomass by-products get processed to make fuels or useful products. EFB and OPF are already used in furniture, building, electronics, packing and automobile industry, but most of them are still used as soil conditioner in plantations /18, p.2414/. Although the planting of oil palms has many advantages compared to other oil delivering plants, it has its disadvantages as well. Due to clearing of rainforest areas, especially in Malaysia and Indonesia, and the accompanied proliferation of monocultures it threatens animal species, like the orang-utan, and expels natives from their homeland. There are reports of forced and child labour on plantations in Indonesia, which might be one of the reasons of the low price of palm oil /19, p. 6; 8–11/. Unfortunately it is still cheaper to use cleared rainforest areas instead of improving

the exploitation of existing ones. As an example the peaterys, which are big CO₂ storages, are dried and the CO₂ is released into the atmosphere /20/ 21, p. 6/.

These reasons show why it is necessary to research the use of palm oil production by-products as fuels. This chapter gives an overview of previous OPF pyrolysis experiments. OPF is the mesocarp fibre that is left with the EFB after the oil extraction of the fruits.

4.2. Literature search

Hooi *et al.* /8/ did a laboratory scale pyrolysis of pressed fruit fibres from oil palm. They investigated the effect of the pyrolysis temperature in the range of 450 °C to 800 °C, with an oven dried sample mass of 110 g, at a heating rate of 10 °C·min⁻¹. When the set point temperature was reached, the experiment ran for one hour. The temperature difference between each test was 50 °C and for every temperature three experiments were performed. A fixed bed stainless steel container heated by a muffle oven was used as the reactor. The released gases and vapours were cooled and condensed in in two water cooled condensers, the emerged liquid stored in ice cooled flasks and the non-condensable gases were burned. After the pyrolysis was finished, the char cooled down in the reactor for 24 hours. The obtained results show that the char yield decreased with rising temperature from 34.82 % to 25.89 %. The char had an average ash content of 16.6 % and an average moisture of 5.27 %. The FC increased up to 600 °C and then remained constant, VM showed an opposite trend. Up to 600 °C the HHV increased to a maximum of 27.07 MJ·kg⁻¹ and then remained nearly constant. The maximum liquid yield of 42.03 % was attained at 450 °C, afterwards it decreased to 36.02 % with rising temperature. It was formed by an aqueous and a tarry fraction that was around 40 % of the liquid phase. The HHV of the tarry fraction was 28.35 MJ·kg⁻¹. The gas yield increased with increasing temperature and was calculated by mass difference.

Chen and Lin /1/ investigated the difference of OPF and oil palm fibre pellets (OPFP) pyrolysis in N₂ and CO₂ atmosphere, although CO₂ does not provide an inert atmosphere because it contains oxygen and therefore it is a gasification agent. Dried samples of 20 g were placed in the horizontal quartz reactor with an inner diameter

of 45 mm. The reactor was placed inside a preheated tube furnace at temperatures of 400 °C, 450 °C and 500 °C and kept inside for 30 minutes, with a carrier gas flow rate of 75 mL·min⁻¹. The liquid was collected in an ice cooled flask by condensation of the volatiles, the non-condensable gases were dried by silica gel and analysed. The char yield decreased with increasing temperature and was in the range of 31.9 % to 39 %. In a CO₂ atmosphere, the char yield was always higher than in N₂ atmosphere and OPFP yielded more char than OPF. The HHVs of the char increased with increasing temperature. OPF in CO₂ atmosphere showed the highest HHV, its range was from 18.9 MJ·kg⁻¹ till 21.32 MJ·kg⁻¹. The liquid yield showed the same properties like the solid yield except of the temperature dependence. It ranged from 33.9 % to 40.9 % with a maximum at 450 °C. With CO₂ as a carrier gas and OPFP as the raw material, the HHVs of the liquid phase were smaller than the ones produced with N₂ as the carrier gas and with OPF as raw material. The range was from 7.46 MJ·kg⁻¹ to 11.81 MJ·kg⁻¹ but always the highest at 450 °C. OPF in N₂ atmosphere at high temperatures gave the highest gas yield; also OPF degradation showed a higher CH₄ concentration than OPFP.

Yang *et al.* /10/ investigated the difference between OPS, OPF and EFB pyrolysis at a final temperature of 1000 °C. In another experiment their objective was the pyrolysis of the palm shell at different temperatures from 300 °C until 1000 °C, in steps of 100 °C. The sample was grounded and sieved to a particle size below 1 mm and 2 g of it was placed inside a vertical quartz tube reactor with the measurements of 390 mm in height, an inner diameter of 38 mm and an outer diameter of 42 mm. N₂ was used as the carrier gas, at a flow rate of 120 mL·min⁻¹. After rendering inert, the sample was heated to the final temperature at a heating rate of 10 °C·min⁻¹ and the process kept on going for 30 minutes afterwards. The vapour was condensed in a water and an ice bath, the non-condensable gas was filtered by glass wool and dried with silica gel. Gas samples were taken every 5 minutes after the temperature reached 200 °C. The first experiment showed that OPF had the highest char yield (27.62 %) and the lowest gas yield (13.93 %), but the differences between the three materials were below 4 %. The gas phase of the OPF pyrolysis had the highest H₂ and CO₂

concentrations while the OPS had the highest CH₄ concentration. The results of the OPS pyrolysis showed that the gas yield increased with increasing temperature. In the producer gas composition, the CO₂ concentration decreased until 800 °C from 70 % to 35 %, the CO concentration was in the range of 20 % to 26 %, but was slightly lower at lower temperatures. Concentration of H₂ increased with increasing temperature until 800 °C and then it got stable around 40 %. Regarding CH₄ concentration, its maximum was obtained between 500 °C and 600 °C, at around 12 %. With higher temperatures the solid yield decreased and its composition showed less organic compounds. The liquid yield had its maximum at 600 °C with 58.45 % of the dried biomass. It was a mixture of alcohols, phenols, acids, aldehydes, alkanes, ethers, ketones and esters.

Hossain *et al.* /17/ and others carried out a microwave pyrolysis of OPF and they analysed the effects of different microwave powers, final temperatures, particle sizes and N₂ flow rates on the production of H₂. About 30 g of dried sample were placed in a vertical quartz tube with a N₂ inlet at the bottom. For the first study with different particle sizes, the raw biomass was cut to a diameter of 0.5 mm to 0.7 mm and different fibre lengths of less than 1 mm, 1–3 mm, 4–6 mm, 7–9 mm and 10–12 mm. The other parameters were fixed: the microwave power at 500 W, the N₂ flow rate at 800 mL·min⁻¹, the temperature at 550 °C ± 10 °C and the time until the temperature was reached was set to 20 minutes. Results show that the H₂ content in the gas decreased with increasing particle size, from around 30 % to around 15 %, while CH₄ and CO concentration increased. CO₂ concentration was constant with particle sizes below 6 mm, and then decreased with bigger particle sizes. The second investigation was made with different microwave powers from 400–900 W in steps of 100 W, other parameters were fixed to 1–3 mm fibre length, 800 mL·min⁻¹ N₂ flow rate, 550 °C ± 10 °C for the final temperature and a reaction time of 15 minutes. The H₂ concentration increased with higher microwave powers from 20 % to around 35 %, with a maximum at 800 W. CO concentration decreased not steadily, while CO₂ concentration increased with increasing microwave power. CH₄ concentration had its maximum at 600 W. In the third test the temperature was changed between 450 °C

and 700 °C, in steps of 50 °C. The microwave power was kept at 600 W; carrier gas flow rate at 800 mL·min⁻¹ and particle size was 1–3 mm. The duration of the run varied with the final temperature. The concentration of H₂ was increasing with increasing temperature and it had a maximum at 650 °C, afterwards it stayed nearly stable. CO₂ content increased too, while CO and CH₄ concentrations decreased unsteadily. For the last experiment the N₂ flow rates were adjusted between 200 and 1200 mL·min⁻¹, in steps of 200 mL·min⁻¹, while the microwave power stayed at 600 W, the particle size was 1–3 mm, the final temperature set to 550 °C ± 10 °C and the reaction time was set at 15 minutes. In the results the H₂ content showed an increase until a N₂ flow rate of 1000 mL·min⁻¹, and then seemed to be steady around 30 %. CO and CH₄ concentrations decreased with increasing flow rates, while the CO concentration was increasing. The char yield also decreased with increasing flow rates.

5. EXPERIMENTAL PART

5.1. Characterisation of the raw material

The raw material used in all the tests was frozen OPF supplied from Columbia (Figure 5.2). It was left in the open air to defreeze and dry. Before every experiment the sample was dried in an oven at 105 °C until it had constant weight. Its properties were determined according to different standards and for all properties at least two measurements were performed to calculate an average. Table 5.1 shows the determined properties and a comparison with the properties from /1, p.572, Table 2/.

The oil content was determined according to EN ISO 734-1 2000, the ash content following EN 14775 and the moisture content following EN 14774-3. The average adb-moisture content was 10.8 %. The HHV was determined according to ASTM E711-87 2004 in a Parr oxygen bomb calorimeter, with a Parr 6772 calimetric thermometer that gives the HHV in cal·g⁻¹. For the determination of the VM, a TG analyser type Netsch STA 449 F3 Jupiter was used (see appendix A.2.)

Table 5.1: Properties of OPF, comparison between the determined and values from literature.

Property	Determined	Values from literature /1/
Oil content [wt-%]	2.52	–
HHV [cal·g ⁻¹]	4428.50	–
HHV [MJ·kg ⁻¹]	18.56 (db)	15.38
Cellulose content [wt-%]	–	46.63
Hemicellulose content [wt-%]	–	19.98
Lignin content [wt-%]	–	10.92
Other [wt-%]	–	21.63
Ash [wt-%]	4.22	6.06
VM [wt-%]	78.48	71.49
FC (by difference) [wt-%]	17.30	19.18
C [wt-%]	49.3 (db)	40.21 (db)*
H [wt-%]	6.1 (db)	5.17 (db)*
N [wt-%]	1.0 (db)	1.03 (db)*
O (by difference) [wt-%]	39.4 (db)	47.53 (db)*

*Converted from daf to db

For the ultimate analysis the sample was sent to the Centro da Biomassa para Energia (Biomass Centre for Energy, see [Appendix B](#)). The chemical structure of the raw material was identified by Thermo-Electron cooperation Nicolet 6700 Fourier transform infrared spectroscope (FTIR) with matching EZ Omnic software. The results of the FTIR can be seen in [Figure 5.1](#)

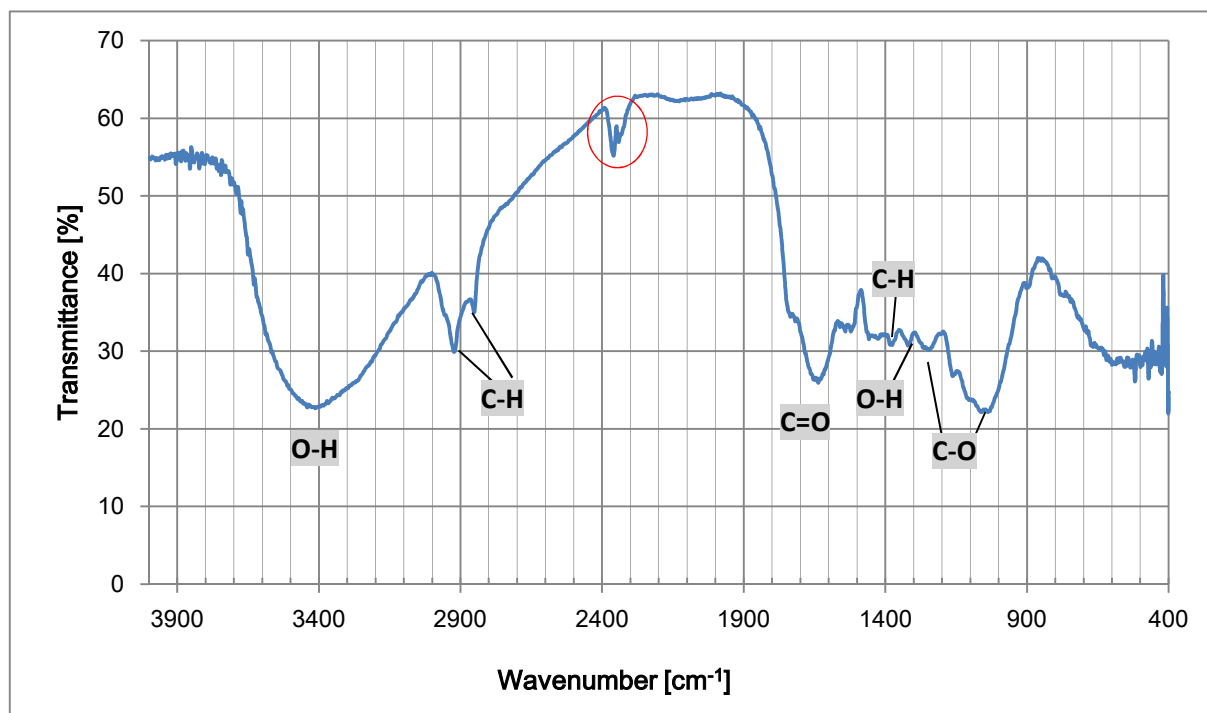


Figure 5.1: FTIR results of raw material with marked peaks.

For the analysis of the graph, [Table 5.2](#) shows the bounds with the matching wave numbers, the wave numbers are taken from /8, p.585 Table 6/ 23/.

Table 5.2: FTIR results of the raw material.

Wave number [cm ⁻¹]	Wave number range [cm ⁻¹]	Bound	Class of compound
3420	3600–3300	O-H stretching	Polymeric O-H, water impurities
2930	3050–2800	C-H stretching sp ³	Alkyl group
2870	3050–2800	C-H stretching sp ³	Alkane/ alkyl
1650	1750–1650	C=O stretching	Ketones, aldehydes, carboxylic acids, amides
1380	1470–1350	C-H bending sp ³	Alkane
1330	1330–1430	O-H bending	Alcohol/ phenol
1260	1300–950	C-O stretching	Acyl group
1150	1300–950	C-O stretching	Alkoxy group

The red marked double peak is the absorbance of CO₂ in the air. The graph has its biggest peaks at 3420 cm⁻¹, 2930 cm⁻¹, 1650 cm⁻¹ and a double peak at 1150 cm⁻¹. Polymeric O-H is the first peak at a wavenumber of 3420 cm⁻¹, but this peak could

also be due to water impurities in the sample. The second peak at 2930 cm^{-1} is a C-H bond, possibly from an alkyl group. At 1650 cm^{-1} the peak is typical for a C=O bond, which could be from a saturated amide. The last of the big peaks at 1150 cm^{-1} is probably from an alkoxy group.



Figure 5.2: Photograph of OPF.

5.2. Experimental apparatus

The experimental apparatus consisted of a vertical refractory steel reactor with an inner diameter of 97 mm and a height of 780 mm. It was heated by a split furnace with a maximum power of 5000 W, equipped with Kanthal electrical wire resistances. A mesh basket served as the fixed bed sample holder; it was connected to a rod to place it inside the reactor. The N_2 feed was on the top of the reactor and therefore the produced gases streamed out at the bottom and then through the condensing unit. Six connected glass flasks immersed in an ice-water bath formed this condensing unit and the condensables were stored inside of the flasks. Followed by the condensing unit was a silica gel column that dried the non-condensable gases and afterwards they passed a portable gas analyser PG-250. [Figure 5.3](#) shows a schematic diagram of the experimental apparatus. Two thermocouples measured the temperature of the process, one was at the end of the rod to measure the temperature inside the sample (T_i) and the other one was placed in the furnace (T_c) to control the set point temperature (T_{set}). They were connected to a Shimaden MR 13

control unit that controlled and regulated the heating process. Photographs of the experimental apparatus can be seen in [Appendix C](#).

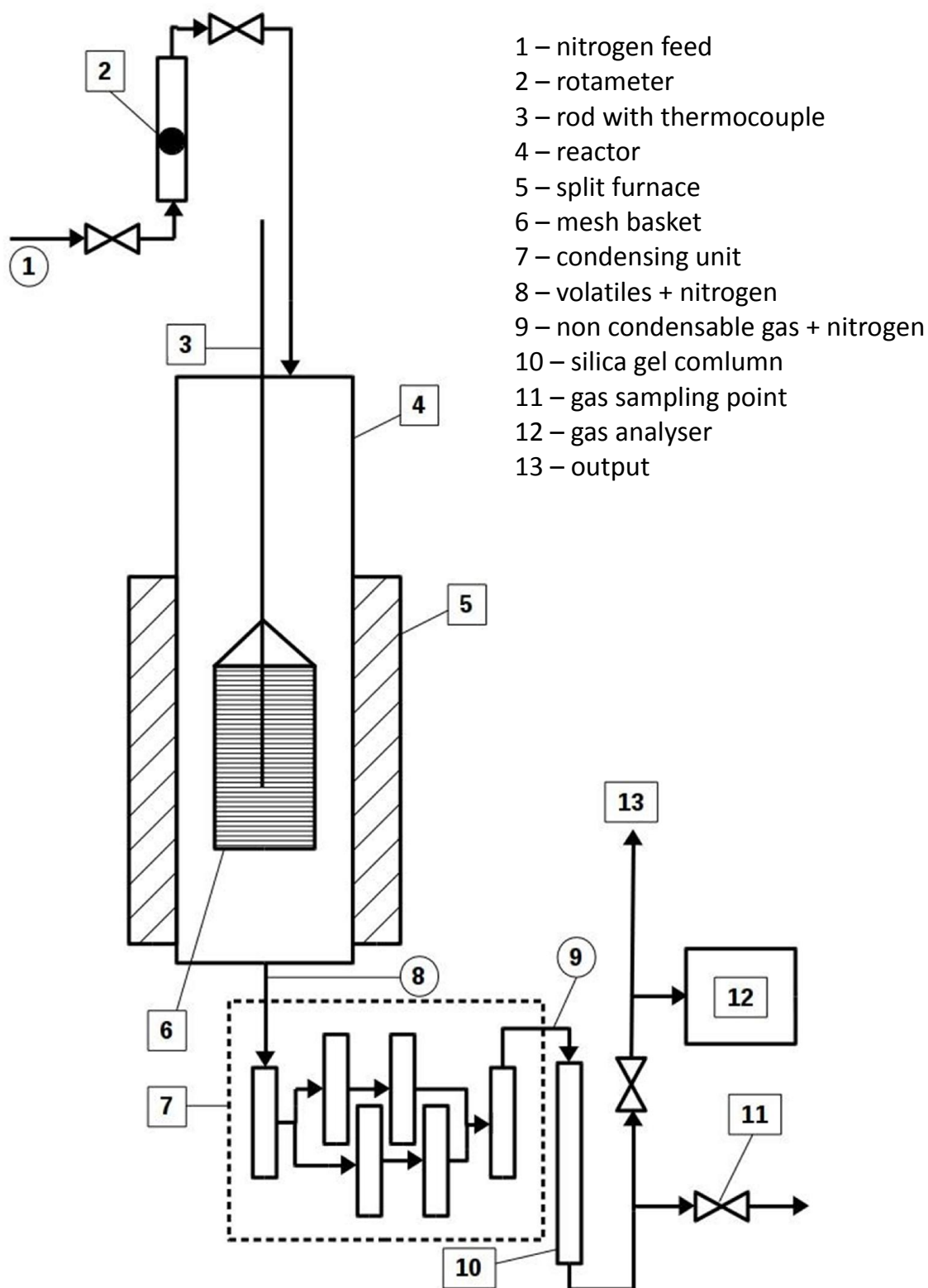


Figure 5.3: Scheme of the reaction system.

5.3. Experimental procedure

The influence of different set-point temperatures from 550–950 °C on the OPF pyrolysis performance and its products was investigated. Temperatures were increased by steps of 100 °C and for each set-point temperature at least two runs were performed to confirm stability in the process parameters, except for 950 °C because there was a leak in the reactor. For each run around 40 g of dry sample were placed inside the mesh basket that was connected to the rod and placed inside the reactor. The N₂ flow rate was adjusted to 2.463 g·min⁻¹. After the inert atmosphere was provided, the heating system was switched on and the heating started from room temperature to the programmed set-point temperature with a heating rate of 20 °C·min⁻¹. The experiments were kept going for at least 15 minutes after the final temperature was reached, then the heating was switched off, while the N₂ continued to flow in order to allow the char to cool down in an inert atmosphere. During each experiment, gas samples were collected in Tedlar bags continuously after the CO concentration started increasing (displayed by the gas analyser) until the end of the experiment.

Before and after every run, the flasks of the condensing unit were weighted to determine the liquid yield from the weight difference. The liquid phase condensed in the connecting tubes was not considered. The liquid phase consisted of an aqueous and a tarry fraction. After weighting, the liquid phase was dissolved with dichloromethane to get it out of the flasks and then the liquids of both runs were mixed together. Afterwards it was centrifuged at 3000 min⁻¹ for ten minutes to separate the aqueous fraction. The remaining liquid was filtered with 5–10 µm filtration paper to get out the small particles and then distilled to separate the bio-oil from the dichloromethane.

The chemical structure of the bio-oil was identified by FTIR apparatus and the HHV was determined.

To determine the solid yield, the basket was weighed before and after the experiment. After removing the char from the basket it was crushed to powder, then the chars of both runs were mixed together and later analysed in a Netzsch STA 449

F3 Jupiter TG analyser. The HHV was also measured. The ash content was determined following EN 14775.

The gas yield was calculated by mass difference. Samples of 1 mL were taken from the various Tedlar bags and were analysed by gas chromatograph (GC). The apparatus used was a DANI GC 1000 equipped with a digital pressure control (DPC), a thermal conductivity detector OPT266 (TCD), an OPT333 injector and a 60/80 Carbonex 1000 column with argon as the carrier gas. For the plotting and the treatment of the results they were edited in the Clarity Lite 4.0.0.876 software (see appendix [A.1.](#)). It gave the concentrations of H₂, O₂, N₂, CO, CO₂ and CH₄. The HHV of the gas phase was calculated from the molar composition by the following equation:

$$\text{HHV} = (30.52 \cdot \text{H}_2 + 30.18 \cdot \text{CO} + 95 \cdot \text{CH}_4) \cdot 4.2 \quad (5-1)$$

With: H₂; CO; CH₄ [vol-%]

$$\text{HHV} [\text{kJ} \cdot (\text{Nm}^3)^{-1}] \quad /24, \text{ p. 119/}$$

6. RESULTS AND DISCUSSION

6.1. Yields of the pyrolysis products

One of the main objectives of this work was to examine the influence of different pyrolysis temperatures on the yields of the products. For the set-point temperatures of 550 °C, 650 °C, 750 °C and 850 °C two runs were performed and an average yield and an average inner temperature were calculated. The maximum difference of all the yields between two runs on the same set-point temperature was 2.2 %. Because of the leak in the reactor, only one experiment was performed at the set-point of 950 °C. In the following graphs and discussions the referred temperature is the inside temperature that is 80–90 °C lower than the set-point temperature. A graph of the dependence of the yields on the temperature inside the reactor can be seen in [Figure 6.1](#).

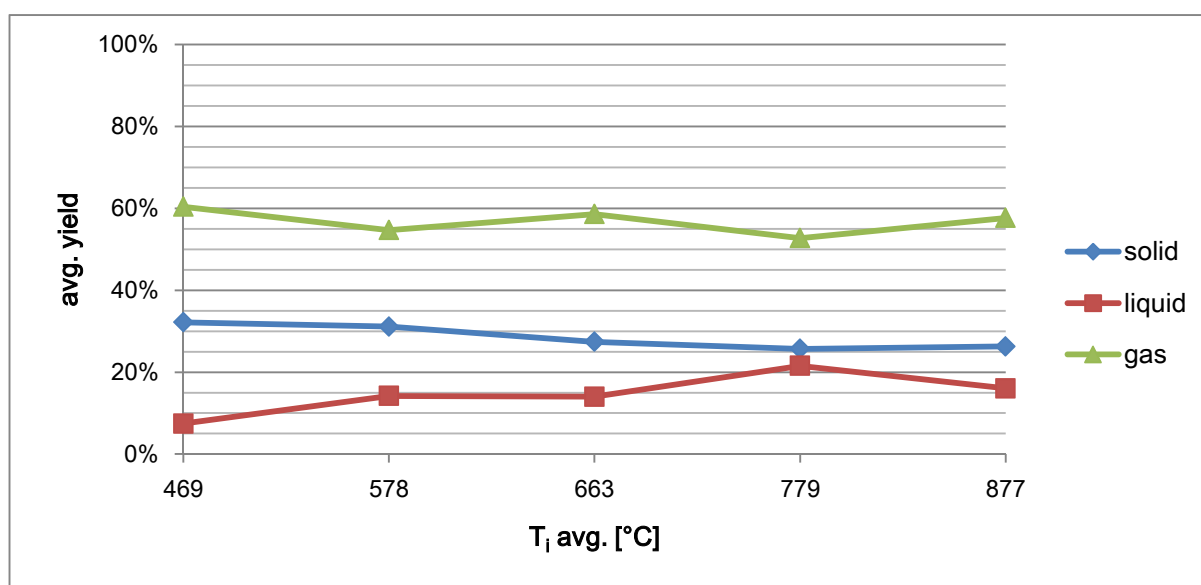


Figure 6.1: Avg. yields of product phases at different avg. inner temperatures.

The maximum of the char yield was 32.2 % at the lowest tested temperature; it steadily decreased until 25.7 % at an inner temperature of 779 °C due to the releasing of volatiles and on-going secondary cracking. The liquid yield increased from 7.4 % at 487 °C to 21.6 % at 779 °C and then decreased to 16.1 %. The gas yield was supposed to increase with increasing temperature (see section [6.3](#).) but it fluctuated between 52.7 % and 60.4 % with its maximum at the lowest temperature. Because the gas

yield was determined by mass difference its behaviour followed the behaviour of the solid and liquid yields.

6.2. Higher heating values of the pyrolysis products

An increase in the HHV of the products compared to the raw material is the main goal of the pyrolysis process. For every HHV three determinations were realised to form an average, except for the HHV determination of liquid phase for the experiments at 650 °C set-point temperature, because there was not enough sample. The maximum difference between two tests of the same sample was $1.63 \text{ MJ}\cdot\text{kg}^{-1}$. A broken tube in the centrifuge caused a sample loss of the liquid from the first experiments, so there was not enough left to determine the HHV. The average HHV of the char was $28.1 \text{ MJ}\cdot\text{kg}^{-1}$ and this value is 51.3 % higher than the HHV of the raw material. For the bio-oil the average HHV was $27.3 \text{ MJ}\cdot\text{kg}^{-1}$, which leads to an increase of 47.1 % compared to the HHV of the raw material. It was useful to take an average increase because [Figure 6.2](#) shows that the HHVs of both product phases are nearly constant around $28 \text{ MJ}\cdot\text{kg}^{-1}$.

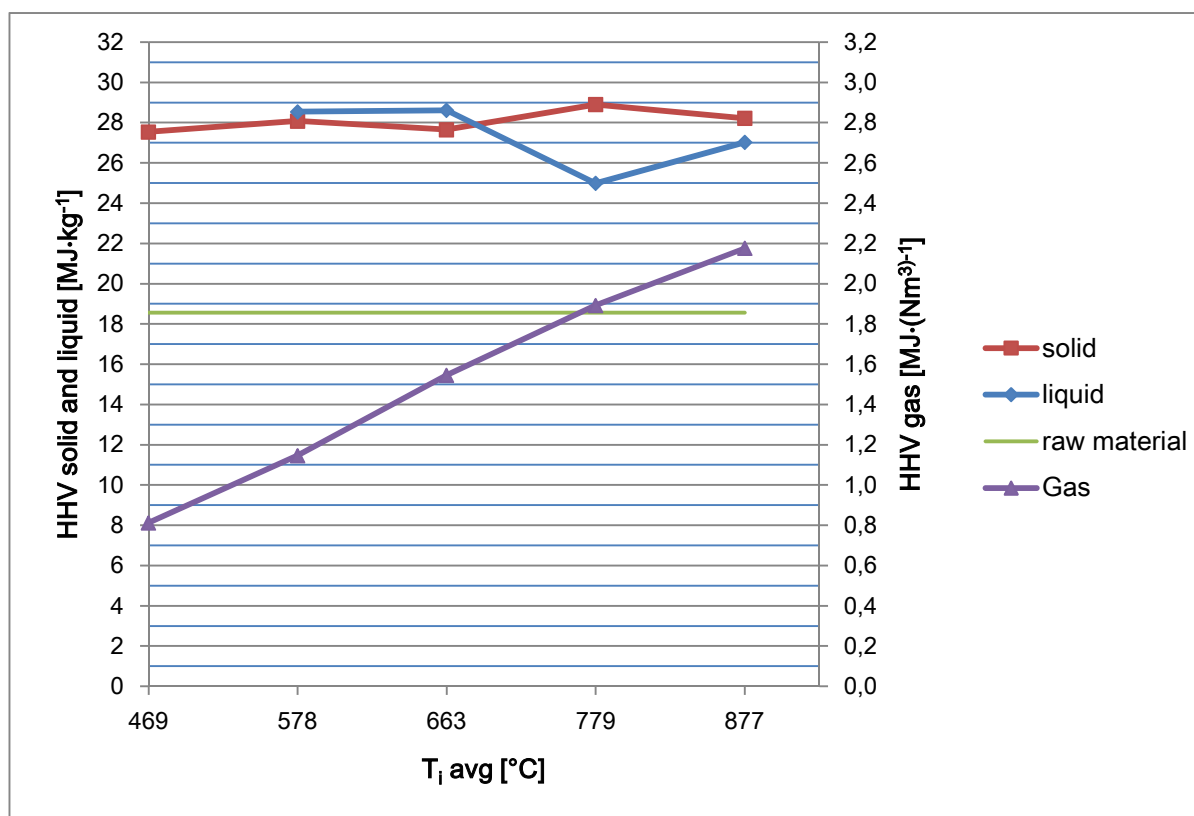


Figure 6.2: HHVs of the product phases according to the avg. inner temperature.

Only for the bio-oil there was a slight decrease to $25 \text{ MJ}\cdot\text{kg}^{-1}$ at $779 \text{ }^\circ\text{C}$. At this temperature the liquid phase had lower viscosity than usual, so maybe after the processing there was still a bit of water in it. In the gaseous phase, the HHVs presented a linear increase with increasing temperature, which may be due to the higher H_2 content (see section 6.3). With a nearly double increase of the inner temperature, the HHV of the gas increased more than two and a half times from $0.8 \text{ MJ}\cdot(\text{Nm}^3)^{-1}$ to $2.2 \text{ MJ}\cdot(\text{Nm}^3)^{-1}$.

Table 6.1 shows the comparison of the present results with other important fuels. It shows that the HHVs of the products were not as high as the ones of traditional fuel. The char seems to have the characteristics to be a potential fuel, but it is not only depending on the HHV but also on the composition and combustion behaviour. For the gaseous phase the HHV was much lower compared to standard gaseous fuels because it was diluted with N_2 .

Table 6.1: HHV of different fuels.

Fuel	HHV (db)	Reference
Solids	$[\text{MJ}\cdot\text{kg}^{-1}]$	
OPF (raw material)	18.56	
OPF char (avg.)	28.1	
charcoal	34.39	/6, p.1056 Table 3/
Anthracite coal	31.84	/6, p.1056 Table 3/
German lignite	25.1	/6, p.1056 Table 3/
Wood	17.7	/2, p.1238 Table 14.6/
Torrefied wood	20.4	/2, p.1238 Table 14.6/
Liquids	$[\text{MJ}\cdot\text{kg}^{-1}]$	
OPF Oil (avg.)	27.3	
Diesel	43.1	/2, p.1430 Table 16.9/
Bio-Diesel	37.1	/2, p.1430 Table 16.9/
Domestic fuel oil	42.8	/2, p.1212 Table 14.3/
Gases	$[\text{MJ}\cdot(\text{Nm}^3)^{-1}]$	
OPF Gas (max)	2.2	
LPG (avg)	117.23*	/25/
Propane	101.32*	/25/

*converted

6.3. Gas phase analysis

The producer gas composition is important to be determined for the calculation of the HHV and the possible usage of the gas. For the calculation of the HHV of the gas (see equation (5-1)) only the determination of the CO, CH₄ and H₂ is necessary, but because it is an interesting factor for the environmental friendliness the CO₂ content was determined too. The following Figure 6.3 shows the amount of produced gas per kg of raw material as a function of the average temperature inside the reactor during the experiments.

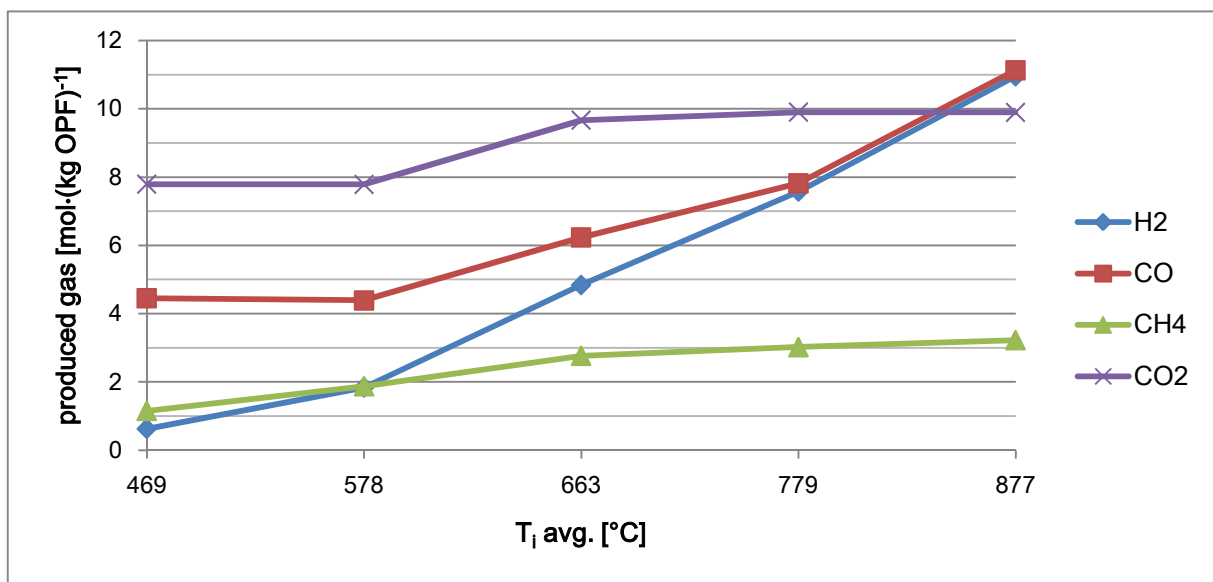


Figure 6.3: Produced gas components according to inner temperature.

With increasing temperature the production of CO and H₂ increased rapidly. For H₂ the slope increased clearly after the inner temperature of 578 °C, while it was 1.84 mol·(kg OPF)⁻¹ at 578 °C it reached 10.96 mol·(kg OPF)⁻¹ at the final inner temperature of 877 °C. So the production was nearly six times higher while the temperature was not even doubling. At lower temperatures CO had a higher production than H₂, its slope increased after 578 °C as well but not as distinctly as the one of H₂. At 469 °C the CO content was 4.45 mol·(kg OPF)⁻¹ and it increased to 11.13 mol·(kg OPF)⁻¹ at 877 °C. Thus its production was two and a half times higher at the final inner temperature of 877 °C. CH₄ and CO₂ concentrations increased with increasing temperature too, but not as rapid as CO and H₂. CH₄ presented a lower

production of $1.15 \text{ mol} \cdot (\text{kg OPF})^{-1}$, but it showed a slight increase at higher temperatures. Until an inner temperature of $663 \text{ }^\circ\text{C}$ the production increased nearly two and a half times, afterwards it was still increasing, but only around 17 % to its maximum of $3.23 \text{ mol} \cdot (\text{kg OPF})^{-1}$ at the final temperature. Because of the increase of these gases with increasing temperature, the HHV of the gas phase was also increasing. CO_2 was steady below $578 \text{ }^\circ\text{C}$ at around $7.8 \text{ mol} \cdot (\text{kg OPF})^{-1}$, then stepped up to $9.7 \text{ mol} \cdot (\text{kg OPF})^{-1}$ and remained nearly constant.

For better understanding of the gas production, [Figure 6.4](#) shows the produced gas in $\text{kmol} \cdot (\text{kg OPF})^{-1}$, without the N_2 content.

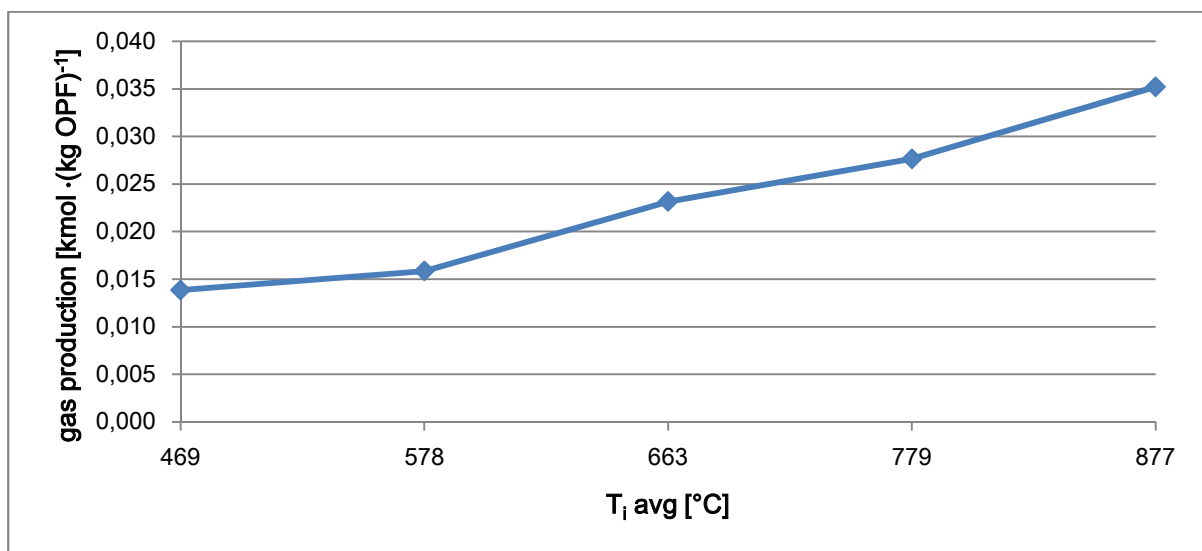


Figure 6.4: Produced gas per kg of raw material according to inner temperature.

As expected in pyrolysis processes, the gas production increased with increasing temperature because more volatiles were released and cracked to non-condensable gases. The initial gas production started around $0.014 \text{ kmol} \cdot (\text{kg OPF})^{-1}$ and increased slowly to $0.016 \text{ kmol} \cdot (\text{kg OPF})^{-1}$ at $578 \text{ }^\circ\text{C}$ inner temperature. Afterwards it increased up to $0.035 \text{ kmol} \cdot (\text{kg OPF})^{-1}$ at the highest inner temperature of $877 \text{ }^\circ\text{C}$, so it was more than doubling. [Figure 6.4](#) shows that although the gas yield was not increasing, when calculated by mass difference, in fact the gas production increased with higher temperature. The gas yield was only calculated to show the trend of the gas production, due to the oscillation of the float of the rotameter. So it was difficult to put the float exactly in position “3” (corresponding to $2.463 \text{ g} \cdot \text{min}^{-1}$), therefore the numbers of the calculated results may vary but the trend stays the same.

6.4. Char analysis

The TG analysis of the char gave results for the VM on a dry basis. The db-ash content was determined separately due to problems in the TG during the air-injection (see appendix A.2.). The FC was calculated by mass difference. The results are on a dry basis and are shown in [Figure 6.5](#).

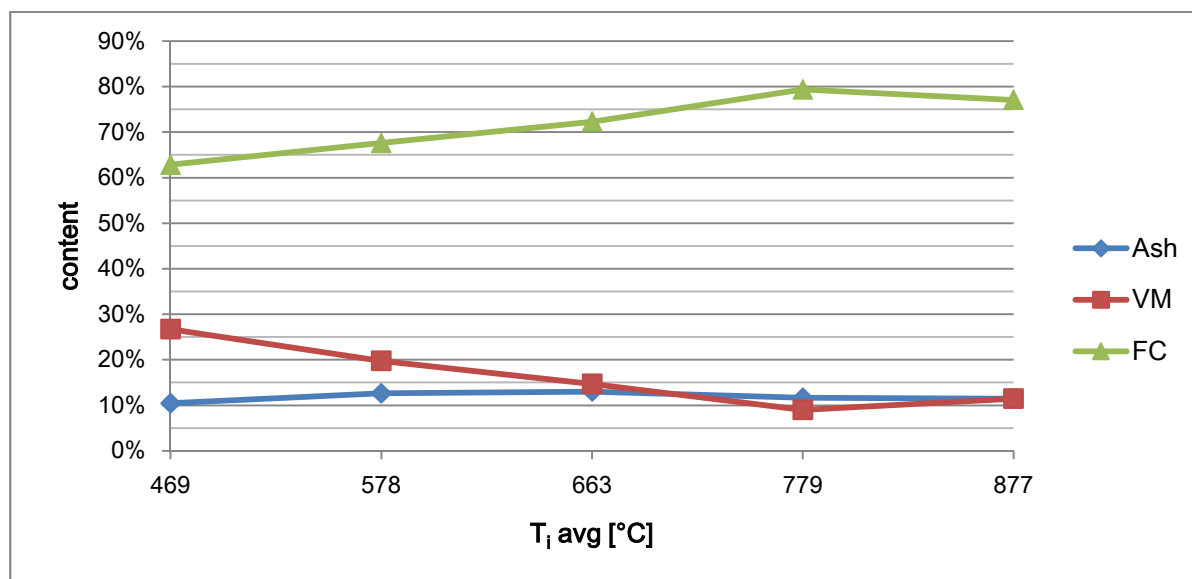


Figure 6.5: FC, VM and ash of the char at different temperatures.

The ash content of the solid phase was nearly constant at all temperatures. It varied between 10 % at an inner temperature of 469 °C and 13 % at 663 °C, and it did not show a dependence on the temperature. The average ash content was 12%. As expected, the VM showed a decrease with increasing temperature; this is due to more volatiles released at higher temperatures. It decreased from 27 % at the first temperature until 9 % at 779 °C. Afterwards, it showed a small increase to 11 % but it is supposed to be stable with higher temperatures, slight differences may be due to fluctuating properties of the biomass. The TG analysis should be repeated, because there was a difference in the results obtained for similar conditions. This could be justified by a malfunction of the N₂ generator. There was no time for repeating the tests, but the results show the estimated trend. The FC increased with higher temperatures, this may be due to more volatiles released at higher temperatures. Because of the stable ash content, the FC went along with the VM trend. It started at 63 % and increased until 79 % at 779 °C. At the last temperature, it showed a small decrease to 77 %.

6.5. Liquid phase analysis

The bio-oil was analysed by FTIR. [Figure 6.6](#) shows the results of all the bio-oil obtained at different pyrolysis temperatures. The graphs have the same peaks, only their transmittance varies. The wavenumbers from 400 cm^{-1} to 600 cm^{-1} are cut out because the NaCl pellets that carried the sample defiled the graph in the first wave numbers. The labels used for each curve refer to the set-point temperature of the particular experiment.

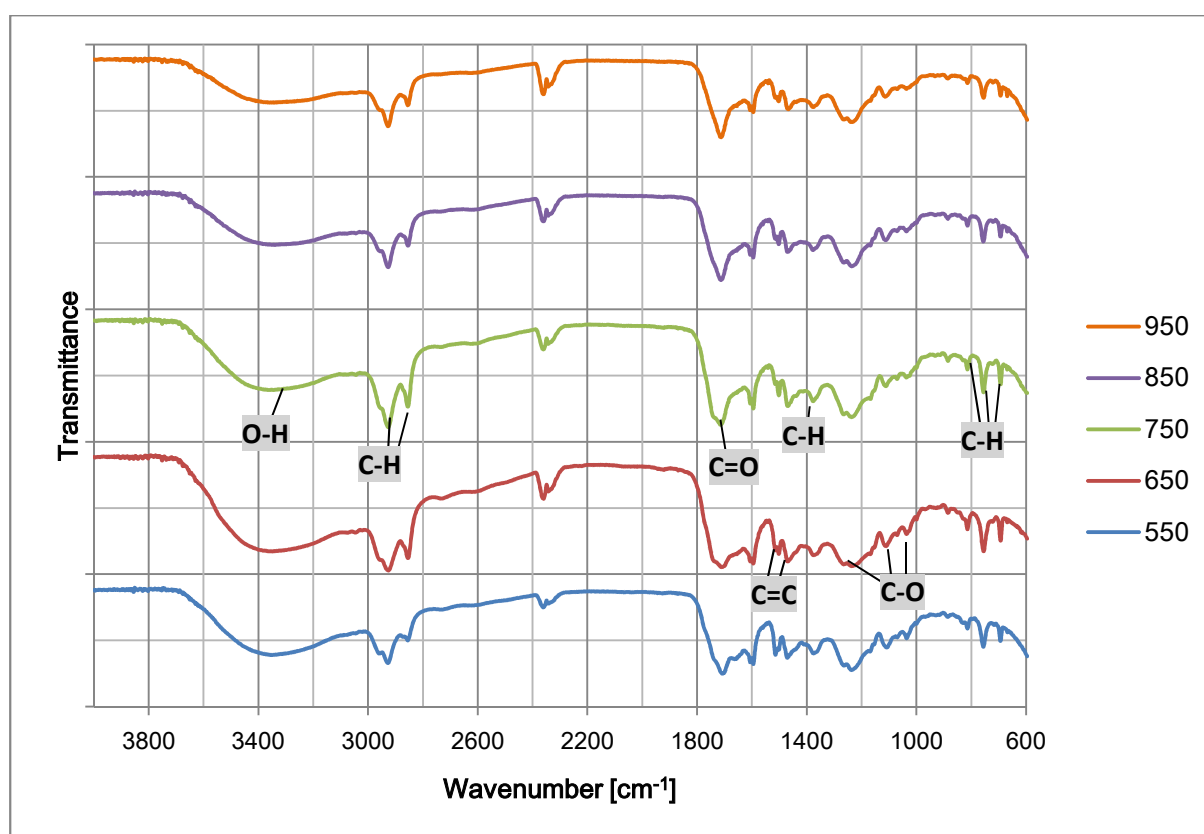


Figure 6.6: FTIR results of all experiments.

The first peak at around 3350 cm^{-1} was an O-H stretching, which could be from an alcohol or a carboxylic acid; it could also be water impurities because the water was taken out with a pipette, so it was hard to know if all the water was taken out. At 2930 cm^{-1} and 2870 cm^{-1} the peaks were from C-H stretching, which could be from an aldehyde. Like in the raw material, the peak in the middle around 2630 cm^{-1} was from CO_2 in the atmosphere. The peak at 1720 cm^{-1} was from a C=O stretching, possibly from a ketone ring or an aromatic ester. An aromatic C=C stretching was the reason for the next two peaks at 1520 cm^{-1} and 1480 cm^{-1} . They were followed by three C-O stretches at 1250 cm^{-1} , 1120 cm^{-1} and 1050 cm^{-1} , while the one at 1250 cm^{-1} was from

an acyl group, the other two were from alkoxy groups. The last three peaks at 820 cm^{-1} , 780 cm^{-1} and 700 cm^{-1} were from C-H bending from an aromatic compound or alkene. The results are summarised in [Table 6.2](#), they are compared with data from /8, p.585 Table 6/ 23/.

Table 6.2: FTIR results for the charts compared with the literature.

Wave number of peak [cm^{-1}]	Wave number range [cm^{-1}]	Bound	Class of compound
3350	3600–3300	O-H stretching	Carboxylic acid, alcohols, water impurities
2930	3050–2800	C-H stretching sp^3	Alkyl group
2870	3050–2800	C-H stretching sp^3	Alkane, alkyl
1720	1750–1650	C=O stretching	Ketones, aldehydes, carboxylic acids, amides
1520	1480–1650	C=C stretching	Aromatic
1480	1480–1650	C=C stretching	Aromatic
1380	1470–1350	C-H bending sp^3	Alkane
1250	1300–950	C-O stretching	Acyl group
1120	1300–950	C-O stretching	Alkoxy group
1050	1300–950	C-O stretching	Alkoxy group
820	650–1000	C-H bending sp^2	Aromatic, alkene
780	650–1000	C-H bending sp^2	Aromatic, alkene
700	650–1000	C-H bending sp^2	Aromatic, alkene

7. SUMMARY AND CONCLUSIONS

The pyrolysis experiments of OPF with different set-point temperatures from 550 °C to 950 °C were performed in a fixed bed steel reactor with a split furnace.

The liquid yield had its maximum with 21.6 % at an inner temperature of 779 °C which is not an expected behaviour, since normally its maximum is around 450–500 °C. With higher temperature the secondary cracking starts and cracks some condensable gases into non-condensable gases. The bio-oil consisted of a lot of compounds like carboxylic acid, ketones, aldehydes, alcohols, alkenes, aromatic compounds, acyl and alkoxy groups as observed by FTIR. The HHV of the water-free liquid was between 27 MJ·kg⁻¹ and 29 MJ·kg⁻¹ only at 779 °C it had a small decrease. It is 47 % higher than the HHV of the raw material. After treatment the liquid can be used to produce chemical compounds or maybe as a fuel. For the solid phase, the yield was between 25 % and 32 % and it decreased with rising temperatures. The HHV of the solid residue was between 27 MJ·kg⁻¹ and 29 MJ·kg⁻¹ with an average of 28.1 MJ·kg⁻¹, so it was 51 % higher than the HHV of the raw material. Different analyses were performed to get the FC, VM and ash content of the char. The VM decreased when the bed temperature increased, the ash content remained nearly constant, around 11 %. Because the FC was calculated by mass difference, it went along with the VM but it showed the opposite trend. The solid phase can be processed to activated carbon or for soil remediation. The gas yield was also calculated by mass difference; therefore it fluctuated around 55 %. The gas composition showed an increase in H₂ content, with increasing temperatures it is nearly six times higher at the highest tested temperature than at the lowest. The maximum obtained value was 10.96 mol·(kg OPF)⁻¹. The concentration of CO also showed a rapid increase, while CO₂ and CH₄ concentration only showed a small increase at higher temperatures. With the higher H₂ content at higher temperatures, the HHV of the gas also increased with higher temperatures. Its maximum obtained value was 2.2 kJ·(Nm³)⁻¹ at the highest tested temperature of 877 °C and it was over two times higher than at the lowest temperature. But it was still lower than

conventional fuels because it was diluted with N₂. None of the pyrolysis products had a comparable HHV to fossil fuels.

For future work, the influence of other process parameters, like the heating rate or the carrier gas flow rate should be investigated to see if they affect the pyrolysis products.

REFERENCES

- /1/ W.H. Chen, B.J. Lin **“Characteristics of products from the pyrolysis of oil palm fiber and its pellets in nitrogen and carbon dioxide atmospheres”** Elsevier, Energy Vol. 94, 2016, p. 569–578
- /2/ M. Kaltschmitt, H. Hartmann, H. Hofbauer **“Energie aus Biomasse: Grundlagen, Techniken und Verfahren”** 3rd edition, Springer-Vieweg, 2016, ISBN: 978-3-662-47438-9
- /3/ P. Basu **“Biomass gasification and pyrolysis: practical design”** academic press by Elsevier Inc., 2010, ISBN: 978-0-12-374988-8
- /4/ V. Dhyani, T. Bhaskar **“A comprehensive review on the pyrolysis of lignocellulosic biomass”** Elsevier, Renewable Energy, 2017, p. 1–22
- /5/ Dr. U. Bauermeister **“Vorlesung Biomasseverwertung” (lecture of biomass utilisation)** University of applied sciences Merseburg, winter term 2015/16
- /6/ S.A. Channiwala, P.P. Parikh **“A unified correlation for estimating HHV of solid, liquid and gaseous fuels”** Elsevier, Fuel Vol.81, 2002, p. 1051–1063
- /7/ P. Weerachanchai, C. Tangsathitkulchai, M. Tangsathitkulchai **“Characterization of products from slow pyrolysis of palm kernel cake and cassava pulp residue”** Korean J. Chem. Eng. Vol. 28(12), 2011, p. 2262–2274, DOI: 10.1007/s11814-011-0116-3
- /8/ K.K. Hooi, Z.A.Z. Alauddin, L.K. Ong **“Laboratory-scale pyrolysis of oil palm pressed fruit fibres”** Journal of Oil Palm Research Vol. 21, June 2009, p. 577–587
- /9/ J.F. González, J.M. Encinar, J. L-Canito, E. Sabio, M. Chacón **“Pyrolysis of cherry stones: energy uses of the different fractions and kinetic study”** Elsevier, Journal of Analytical and Applied Pyrolysis Vol. 67, 2003, p. 165–190
- /10/ H. Yang, R. Yan, H. Chen, D.H. Lee, D.T. Liang, C. Zheng **“Mechanism of Palm Oil Waste Pyrolysis in a Packed Bed”** Energy & Fuels Vol. 20, 2006, p. 1321–1328

- /11/ N.B. Alias, N. Ibrahim, M.K.A. Hamid, H. Hasbullah, R.R. Ali, R.M. Kasmani **“Investigation of oil palm wastes’ pyrolysis by thermo-gravimetric analyzer for potential biofuel production”** Elsevier, Energy Procedia Vol. 75, 2015, p. 78–83
- /12/ D. Neves, H. Thunman, A. Matos, L. Tarelho, A. Gómez-Barea **“Characterization and prediction of biomass pyrolysis products”** Elsevier, Progress in Energy and Combustion Science Vol. 37, 2011, p. 611–630
- /13/ G. Chang, Y. Huang, J. Xie, H. Yang, H. Liu, X. Yin, C. Wu **“The lignin pyrolysis composition and pyrolysis products of palm kernel shell, wheat straw, and pine sawdust”** Elsevier, Energy Conversion and Management Vol. 124, 2016 p. 587–597
- /14/ J. Cho, J.M. Davis, G.W. Huber **“The Intrinsic Kinetics and Heats of Reactions for Cellulose Pyrolysis and Char Formation”** Wiley-VCH Verlag GmbH & Co. KGaA, Weinheim, ChemSusChem Vol. 3, 2010, p. 1162 – 1165, DOI: 10.1002/cssc.201000119
- /15/ H. Yang, R. Yan, H. Chen, D.H. Lee, C. Zheng **“Characteristics of hemicellulose, cellulose and lignin pyrolysis”** Elsevier, Fuel Vol. 86, 2007, p. 1781–1788
- /16/ A.R. Mohameda, Z. Hamzaha, M.Z.M. Daud, Z. Zakaria **“The Effects of Holding Time and The Carrier Nitrogen Gas Flow rates On The Pyrolysis Of EFB Using A Fixed Bed Reactor”** Elsevier, Procedia Engineering Vol. 53, 2013, p. 185–191
- /17/ M.A. Hossain, J. Jewaratnam, P. Ganesan, J.N. Sahu, S. Ramesh, S.C. Poh **“Microwave pyrolysis of oil palm fiber (OPF) for hydrogen production: Parametric investigation”** Elsevier, Energy Conversion and Management Vol. 115, 2016, p. 232–243
- /18/ S. Sumathi, S.P. Chai, A.R. Mohamed **“Utilization of oil palm as a source of renewable energy in Malaysia”** Elsevier, Renewable and Sustainable Energy Reviews Vol. 12, 2008, p. 2404–2421
- /19/ R. Behrend, A. Hülsmeier, G. Rodríguez, K. Schenck, C. Zander **“Regenwald Report”** Rettet den Regenwald e.V./regenwald.org, Vol.3, 2013

- /20/ **<http://www.regenwald-statt-palmoel.de/de/palmoel/palmoelproblematik>**
Aktionsbündnis Regenwald statt Palmöl, 2017
- /21/ A. Petry **“Palmöl: Fluch oder Segen? Wie ein Rohstoff Klima und Regenwald bedroht und dennoch auf eine grünere Zukunft hoffen lässt”** WWF Germany, 2012
- /22/ M. Carrier, T. Hugo, J. Gorgens, H. Knoetze **“Comparison of slow and vacuum pyrolysis of sugar cane bagasse”** Elsevier, Journal of Analytical and Applied Pyrolysis Vol. 90, 2011, p. 18–26
- /23/ **http://www.cpp.edu/~psbeauchamp/pdf/424_spectra_tables.pdf** accessed july 2017
- /24/ A.F. Almeida, I.M. Pereira, P. Silva, M.P. Neto, A.C. Crispim, R.M. Pilão, A.M. Ribeiro **“Pyrolysis of Leather Trimmings in a Fixed Bed Reactor”** JALCA, Vol. 112, 2017, p. 112–120
- /25/ **http://www.engineeringtoolbox.com/gross-net-heating-values-d_420.html** accessed june 2017

APPENDIX A: CALCULATIONS

A.1. Calculation of the gas composition

The Clarity Lite 4.0.0.876 software gives a graph for every analysis. [Figure A.1](#) gives an example of the different curves obtained during the analysis of a gas sample from the pyrolysis experiment at a set-point temperature of 550 °C. For every graph the peaks of H₂, O₂, N₂, CO, CH₄ and CO₂ were selected and their area was given by the software. O₂ and N₂ build a double peak that is hard to see in this picture.

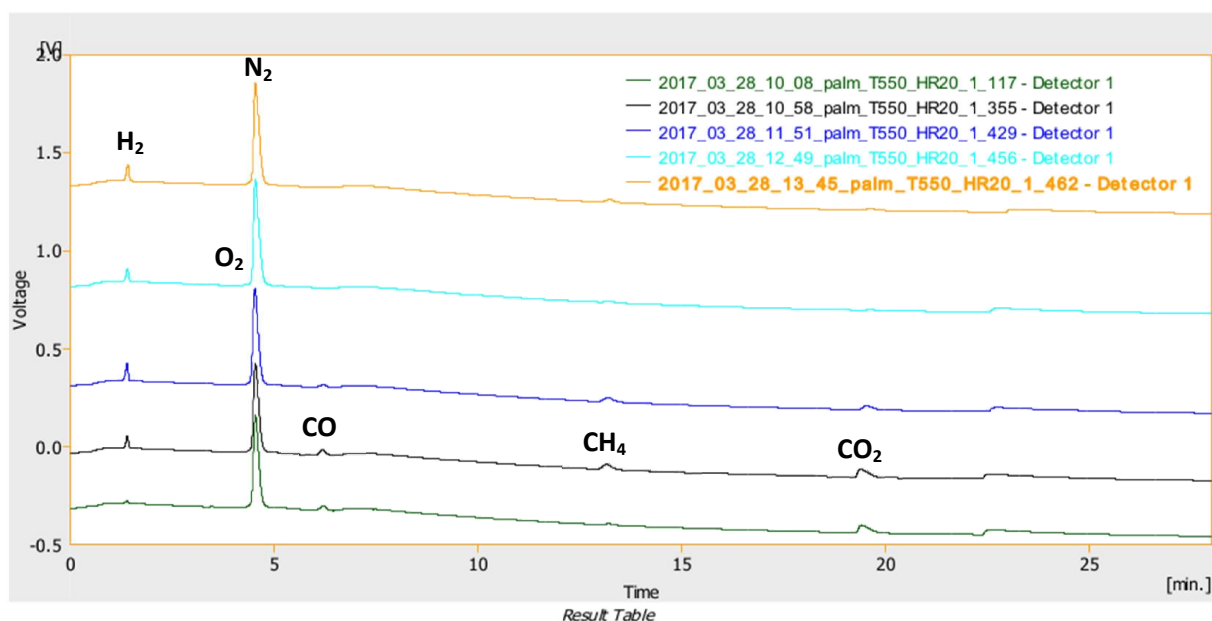


Figure A.1: Example (set-point temperature of 550 °C) for different GC-TCD chromatogram curves in one picture, with matching table for the first curve.

For every gas component, a previous calibration of the GC was performed and the calibration curves are shown in [Table A.1](#). This table also gives the ranges of the peak retention times for every component. With the calibration curves and the areas from [Figure A.1](#) the mass concentration of every component can be calculated for every run. The mass concentration is then divided by the density of the gas (at 20 °C and 1 bar) to get the volume percentage of every gas. For every gas sample an average

time between start and end time of the sampling was calculated to get the time difference between two gas samples of the same experiment.

Table A.1: Density, peak times and calibration curves of gas components.

Component	Density* [mg/cm ³]	Time of peak appearance [min]	Calibration curve
H ₂	0.083	1.36–1.55	$c = \frac{\text{area}+127.30}{653108.70}$; R ² =0.9998
O ₂	1.33	4.42–4.46	$c = \frac{\text{area}+19.16}{4195.85}$; R ² =0.9957
N ₂	1.165	4.50–4.60	$c = \frac{\text{area}-7.98}{4652.84}$; R ² =0.9995
CO	1.165	6.16–6.25	$c = \frac{\text{area}+29.37}{4206.96}$; R ² =0.9984
CH ₄	0.666	13.17–13.29	$c = \frac{\text{area}+26.36}{28237.92}$; R ² =0.9997
CO ₂	1.83	19.44–19.71	$c = \frac{\text{area}+31.99}{3290.93}$; R ² =0.9980

* at 20 °C and 1 bar

Example: Hydrogen, for a test at a set-point temperature of 550 °C

Start time of gas sample: 24:22 min = t_{start}

End time of gas sample: 30:33 min = t_{end}

Average time: 1647 s

Sample mass (OPF) 0.03762 kg = m_s

$$c_{H_2} = \frac{A_{H_2}+127.30}{653108.70} = \frac{67.285 \text{ mVs}+127.30}{653108.70} = \underline{0.0003 \frac{\text{mg}}{\text{ml}}} \quad (\text{A-1})$$

$$c_{V_{H_2}} = \frac{c_{H_2}}{\rho_{H_2}} \cdot 100 \% = \frac{0.0003 \frac{\text{mg}}{\text{ml}}}{0.083 \frac{\text{mg}}{\text{cm}^3}} \cdot 100 \% = \underline{0.36 \text{ vol-}\%} \quad (\text{A-2})$$

With: c_{H₂} – mass concentration of H₂ [mg·mL⁻¹]

c_{V_{H₂}} – volume concentration of H₂ [vol-%]

A_{H₂} – area of H₂, see table in [Figure A.1](#)

ρ_{H₂} – density of H₂ at 20 °C and 1 bar [mg·mL⁻¹]

With these calculations the volume percentage of H₂ in the first gas sample was determined. The concentration was given per millilitre because 1 mL of sample for every gas bag was injected in the GC.

For further calculations it is important to know the entire gas production, therefore the concentration of N₂ is needed:

$$\dot{n}_{N_2\text{start}} = 1.466 \cdot 10^{-6} \frac{\text{kmol}}{\text{s}}$$

$$c_{N_2} = \frac{A_{N_2} - 7.98}{4652.84} = \frac{4284.711 \text{ mVs} - 7.98}{4652.84} = \underline{0.9192 \frac{\text{mg}}{\text{ml}}} \quad (\text{A-3})$$

$$c_{V_{N_2}} = \frac{c_{N_2}}{\rho_{N_2}} \cdot 100 \% = \frac{0.9192 \frac{\text{mg}}{\text{ml}}}{1.165 \frac{\text{mg}}{\text{cm}^3}} \cdot 100 \% = \underline{78.9 \text{ vol-}\%}$$

With: $\dot{n}_{N_2\text{start}}$ – initial molar flow rate of N_2 , by calibrated flow meter [$\text{kmol}\cdot\text{s}^{-1}$]
 c_{N_2} – mass concentration of N_2 [$\text{mg}\cdot\text{mL}^{-1}$]
 A_{N_2} – area of N_2 , see table in [Figure A.1](#)
 $c_{V_{N_2}}$ – volume concentration of N_2 [vol-%]
 ρ_{N_2} – density of N_2 at 20 °C and 1 bar [$\text{mg}\cdot\text{mL}^{-1}$]

Because no N_2 was produced and the ultimate analysis shows 1 % of N_2 in the raw material (considered negligible), the value obtained for volume percentage of N_2 (78.9 %) refers to $1.466\cdot 10^{-6} \text{ kmol}\cdot\text{s}^{-1}$. To get the complete produced gas flow, the initial molar flow rate had to be divided by the percentage of N_2 in each bag.

$$\dot{n}_g = \frac{\dot{n}_{N_2\text{start}}}{c_{V_{N_2}}} = \frac{1.466\cdot 10^{-6} \frac{\text{kmol}}{\text{s}}}{0.789} = \underline{1.859 \cdot 10^{-6} \frac{\text{kmol}}{\text{s}}} \quad (\text{A-4})$$

With: \dot{n}_g – molar flow rate of the entire gas produced [$\text{kmol}\cdot\text{s}^{-1}$]

To get the molar flow rate of H_2 (or other components) for each sample, the volume percentage of H_2 has to be multiplied by the total gas molar flow rate.

$$\dot{n}_{H_2} = \dot{n}_g \cdot c_{V_{H_2}} = 1.859 \cdot 10^{-6} \frac{\text{kmol}}{\text{s}} \cdot 0.0036 \text{ vol-}\% = \underline{6.655 \cdot 10^{-9} \frac{\text{kmol}}{\text{s}}} \quad (\text{A-5})$$

With: \dot{n}_{H_2} – molar flow rate of H_2 [$\text{kmol}\cdot\text{s}^{-1}$]

According to the trapezoidal rule, an integration of the change in the molar flow over the time gives the total number of moles of a component:

$$n_i = \int_{t_{\text{start}}}^{t_{\text{end}}} d\dot{n}_i \cdot dt \quad (\text{A-6})$$

$$n_g = \underline{0.0027 \text{ kmol}}$$

$$n_{H_2} = \underline{5.48 \cdot 10^{-6} \text{ kmol}}$$

With: n_i – total number of moles for each component for one bag [kmol]
 \dot{n}_j – molar flow rate for every component [kmol·s⁻¹]
 n_g – total number of moles of the entire gas for one bag [kmol]
 n_{H_2} – total number of moles of H₂ for one bag [kmol]

These calculations were only done for one gas sample, because there are more bags per experiment. These calculations have to be done for every gas bag and then add up to get a total for every experiment.

$$n_{i,\text{total}} = \sum_i^m n_i \quad (\text{A-7})$$

$$n_{g,\text{total}} = \underline{0.0054 \text{ kmol}}$$

$$n_{H_2,\text{total}} = \underline{2.54 \cdot 10^{-5} \text{ kmol}}$$

With: $n_{i,\text{total}}$ – total number of moles for each component of all bags [kmol]
 $n_{g,\text{total}}$ – total number of moles for the entire gas of all bags [kmol]
 $n_{H_2,\text{total}}$ – total number of moles for H₂ of all bags [kmol]

These results can be divided by the initial sample mass to get the gas production per kg of OPF:

$$Y_g = \frac{n_{g,\text{total}}}{m_s} = \frac{0.0054 \text{ kmol}}{0.03762 \text{ kg}} = \underline{\underline{0.1425 \frac{\text{kmol}}{\text{kg}}}} \quad (\text{A-8})$$

$$Y_{H_2} = \frac{n_{H_2,\text{total}}}{m_s} = \frac{2.54 \cdot 10^{-5} \text{ kmol}}{0.03762 \text{ kg}} = \underline{\underline{0.00068 \frac{\text{kmol}}{\text{kg}}}}$$

With: Y_g – yield of entire gas per kg of raw material [kmol·(kg OPF)⁻¹]
 Y_{H_2} – yield of H₂ per kg of raw material [kmol·(kg OPF)⁻¹]

This is done for every experiment; the results of two pyrolysis tests with the same temperature are combined to calculate an arithmetic average. These calculations have to be done for every gas component.

A.2. Treatment of the TG results

In the TG experiments, a small amount of sample (around 5 mg) was heated up at a heating rate of $20\text{ }^{\circ}\text{C}\cdot\text{min}^{-1}$ until $900\text{ }^{\circ}\text{C}$, in a N_2 atmosphere with a N_2 flow rate of $50\text{ ml}\cdot\text{min}^{-1}$. The sample was kept at this temperature for seven minutes and then air was injected to burn the remaining of the sample. Due to a malfunction in the injection system of the air, the ash content could not be determined with the TG technique. Only results for calculating the moisture and volatile content were obtained. The moisture content given by the TG was only important to calculate the VM on a dry basis. It was assumed that the moisture evaporated until a temperature of around $110\text{ }^{\circ}\text{C}$ and the VM evaporated during the rest of the time. The results of the TG are the mass loss over the time and the matching temperatures. The data was recorded every 15 seconds. An example of the most important data recorded is shown as Table A.2.

Table A.2: Section of TG results, example for char from pyrolysis at a set-point temperature of $550\text{ }^{\circ}\text{C}$.

Temperature [$^{\circ}\text{C}$]	Time [min:s]	Mass loss [mg]	Sample mass [mg]
31.575	0	0	7.195
106.682	5:00	0.681	6.514
112.363	5:15	0.689	6.506
899.590	44:15	2.368	4.827
900.050	44:30	2.373	4.822
900.575	51:30	2.446	4.749

Example: Char from pyrolysis at $550\text{ }^{\circ}\text{C}$ set-point temperature.

Initial sample mass: $7.195\text{ mg} = m_s$

It is assumed in this example that the moisture was removed at $112.363\text{ }^{\circ}\text{C}$ because the previous temperature was only $106.682\text{ }^{\circ}\text{C}$. After this time the evaporation of the volatiles started and from the first time it reached $900\text{ }^{\circ}\text{C}$ (at 44:30 minutes) seven minutes were counted until 51:30 minutes.

The sample mass was the initial sample mass minus the mass loss:

$$m_i = m_s - m_l \quad (\text{A-9})$$

With: m_i – sample mass at given time [mg]

m_s – initial sample mass [mg]

m_l – mass loss [mg]

For example: $m_{5:15} = 7.195 \text{ mg} - 0.689 \text{ mg} = \underline{6.506 \text{ mg}}$

With: $m_{5:15}$ – sample mass after 5:15 minutes [mg]

The mass of the moisture was equal to the mass loss till 112.363 °C

$$m_M = m_{l,5:15} = \underline{0.689 \text{ mg}} \quad (\text{A-10})$$

With: m_M – moisture mass [mg]

$m_{l,5:15}$ – mass loss at 5:15 minutes (112.363 °C) [mg]

The moisture content was the moisture mass divided by the initial sample mass:

$$M = \frac{m_M}{m_s} \cdot 100 \% = \frac{0.689 \text{ mg}}{7.195 \text{ mg}} \cdot 100 \% = \underline{9.576 \%} \quad (\text{A-11})$$

With: M – total moisture content [wt-%]

Then, the dry VM mass equals the mass loss from 5:15 minutes until 51:30 minutes:

$$m_{VM} = m_{l,51:30} - m_M = 2.446 \text{ mg} - 0.689 \text{ mg} = \underline{1.757 \text{ mg}} \quad (\text{A-12})$$

With: m_{VM} – mass of volatile matter [mg]

$m_{l,51:30}$ – mass loss at 51:30 minutes (seven minutes after 900 °C is reached)
[mg]

To get the dry VM content the mass of the volatiles has to be divided by the dry mass (the initial sample mass without the mass of the moisture), which equals the sample mass at 5:15 minutes:

$$VM = \frac{m_{VM}}{m_{5:15}} \cdot 100 \% = \frac{1.757 \text{ mg}}{6.506 \text{ mg}} \cdot 100 \% = \underline{\underline{27.00 \%}} \quad (\text{A-13})$$

With: VM – volatile matter content [wt-%]

These calculations were done for the raw material and for the char from every set-point temperature. Two TG runs were performed for every sample to get an average. Figure A.2 shows an example of a typical TG graph.

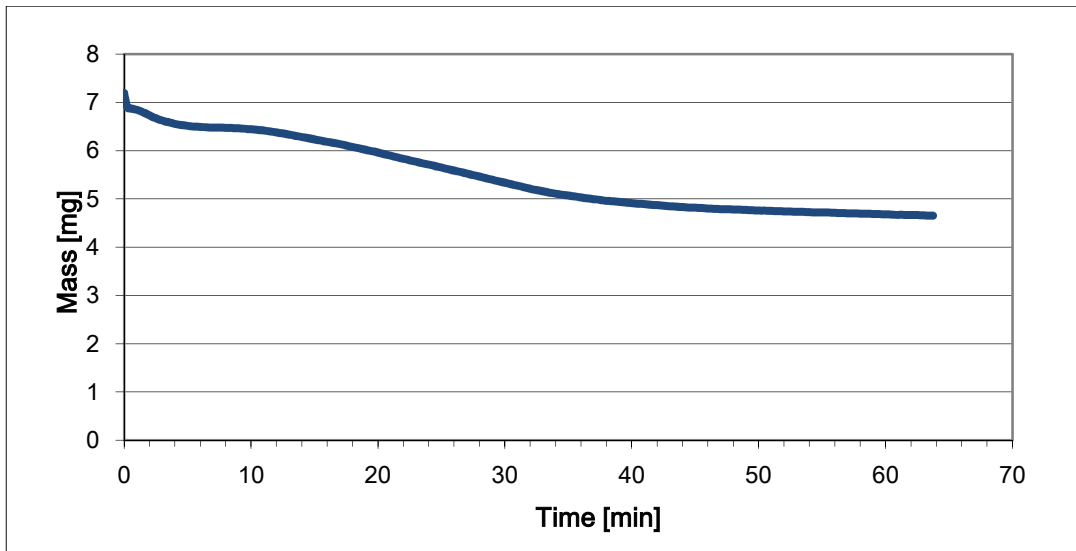


Figure A.2: Example of a TG graph, for the char from the 550 °C pyrolysis.

APPENDIX B: ULTIMATE ANALYSIS RESULTS



Centro da Biomassa para a Energia

Biomass Centre for Energy

LEBS.CBE - Laboratório Especializado em Biocombustíveis Sólidos

BOLETIM DE ENSAIOS Nº 242 /17



AMOSTRA LEBS-CBE Nº 242 /17

Identificação do tipo de amostra:	Biocombustível sólidos - Biomassa
Designação da amostra:	Resíduos de Palma
Análise pedida por:	Instituto Superior de Engenharia do Porto
Endereço:	Rua Dr. António Bernardino de Almeida, 431, 4249-015 Porto
Local de amostragem:	da responsabilidade do cliente
Responsável pela recolha da amostra:	cliente
Data de recepção da amostra:	02-05-2017
Datas de início e de conclusão dos ensaios:	04-05-2017 a 10-05-2017
Data de emissão do boletim de ensaios:	10-05-2017

Reprodução parcial proibida

PARÂMETRO	RESULTADO	UNID.	MÉTODO	OBSERVAÇÕES
Teor de humidade total t_{ic} / Total moisture content a_r	-	% (m/m)	ISO 18134-1:2015	gravimetria
Teor de humidade numa amostra para análise t_{ic} / Moisture general analysis sample a_r	-	% (m/m)	ISO 18134-3:2015	gravimetria
Teor de Cinzas t_{ca} / Ash content d	-	% (m/m)	ISO 18122:2015	gravimetria
Teor de Cinzas t_{ca} / Ash content a_r (1)	-	% (m/m)	ISO 16993:2015	cálculo
Teor de carbono total t_{ct} / Total carbon content d	49,3	% (m/m)	ISO 16948:2015	análise elementar de CHN
Teor de hidrogénio total t_{ht} / Total hydrogen content d	6,1	% (m/m)	ISO 16948:2015	análise elementar de CHN
Teor de azoto total t_{nt} / Total nitrogen content d	1,0	% (m/m)	ISO 16948:2015	análise elementar de CHN
Teor de oxigénio total t_{ot} / Total oxygen content d	-	% (m/m)	ISO 16993:2015	cálculo
Teor de enxofre total t_{st} / Total sulphur content d	-	% (m/m)	ISO 16994:2015	cromatografia iónica
Teor de cloro total t_{ct} / Total chlorine content d	-	% (m/m)	ISO 16994:2015	cromatografia iónica
Poder calorífico superior, volume constante t_{cs} / Gross calorific value, constant volume e	-	MJ/kg	EN 14918:2009	calorimetria
Poder calorífico inferior :				
Poder calorífico inferior, pressão constante t_{ci} / Net calorific value, constant pressure e	-	MJ/kg	EN 14918:2009	cálculo
Poder calorífico inferior, pressão constante t_{ci} / Net calorific value, constant pressure a_r	-	MJ/kg		
Densidade aparente t_{da} / Bulk density e_r	-	kg/m ³	ISO 17828:2015	volumetria / gravimetria
Durabilidade mecânica de peletes / Mechanical durability of pellets	-	% (m/m)	ISO 17831-1:2015	gravimetria
Teor de finos de peletes / Fines content of pellets	-	% (m/m)	EN 15210-1:2009	gravimetria
Comprimento e diâmetro de peletes / Length and diameter of pellets :				
Classe dos peletes / Pellets Class	-	mm		
% de peletes na classe / Class % share	-	% (m/m)		
% de peletes > 40 mm / w% of pellets longer than 40 mm	-	% (m/m)		
Quantidade dos peletes > 40 mm / Number of pellets longer than 40 mm	-	unid.	ISO 17829:2015	análise dimensional
Comprimento médio dos peletes / Mean value of the pellet length	-	mm		
Desvio padrão do comprimento / Standard deviation of the length	-	mm		
Diâmetro médio dos peletes / Average diameter	-	mm		
Desvio padrão do diâmetro / Standard deviation of the diameter	-	mm		
Teor de Arsénio t_{ar} / Arsenic content d (1)	-	mg/kg	ISO 16988:2015	esp. absorção atómica grafite
Teor de Chumbo t_{cb} / Lead content d (1)	-	mg/kg	ISO 16988:2015	esp. absorção atómica grafite
Teor de Cádmio t_{cd} / Cadmium content d (1)	-	mg/kg	ISO 16988:2015	esp. absorção atómica grafite
Teor de Crómio t_{cr} / Chromium content d (1)	-	mg/kg	ISO 16988:2015	esp. absorção atómica grafite
Teor de Cobre t_{cu} / Copper content d (1)	-	mg/kg	ISO 16988:2015	esp. absorção atómica grafite
Teor de Níquel t_{ni} / Nickel content d (1)	-	mg/kg	ISO 16988:2015	esp. absorção atómica grafite
Teor de Zinco t_{zn} / Zinc content d (1)	-	mg/kg	ISO 16988:2015	esp. absorção atómica chama

(continuação)

PARÂMETRO	RESULTADO	UNID.	MÉTODO	OBSERVAÇÕES
Matéria volátil _{lv} / Volatile matter _d (1)	—	% (m/m)	EN 15148:2009	gravimetria
Carbono fixo _{nc} / Fixed Carbon _d (1)	—	% (m/m)	LEBS MI 01	cálculo
Densidade da partícula _q / Particle density _{ar} (1)	—	g/cm ³	ISO 18847:2016	análise dimensional
Comprimento e diâmetro de briquetes / Length and diameter of briquettes (1)	—	mm mm	LEBS MI 02	análise dimensional
Finos de briquetes / Amount of fines for briquettes (1)	—	% (m/m)	LEBS MI 03	gravimetria
Avaliação sensorial / Sensory evaluation (1)	—		LEBS MI 04	
Conteúdo nominal / Nominal content (1)	—	unid.	LEBS MI 05	

GRANULOMETRIAS / PARTICLE SIZE DISTRIBUTION				
Granulometria peletes desintegrados / Particle size dist. disintegrated pellets (ISO 17830:2016) (1)				
Diferença entre massa da amostra e massa total das frações / / Difference mass of test portion and mass of all fractions	—	% (m/m)	P > 3,15 mm	—
			3,15 mm > P > 2,8 mm	—
			2,8 mm > P > 2,0 mm	—
Humidade da amostra peneirada / Moisture content of the sieved sample	—	% (m/m)	2,0 mm > P > 1,4 mm	—
			1,4 mm > P > 1,0 mm	—
			1,0 mm > P > 0,5 mm	—
			0,5 mm > P > 0,25 mm	—
			P < 0,25 mm	—
Granulometria / Particle size distribution (ISO 17827-1:2016) (1)				
			Partículas sobredimensionadas / Hand Sorting > 100 mm	—
Massa total analisada / total mass of test portion	—	g	P > 63 mm	—
Nº de partículas sobredimensionadas / number of overlong	—	unid.	63 mm > P > 45 mm	—
Comprimento da partícula maior / length of longest particle overall	—	mm	45 mm > P > 31,5 mm	—
Diferença entre massa da amostra e massa total das frações / / Difference mass of test portion and mass of all fractions	—	% (m/m)	31,5 mm > P > 16 mm	—
			16 mm > P > 8 mm	—
Humidade da amostra peneirada / Moisture content of the sieved sample	—	% (m/m)	8 mm > P > 3,15 mm	—
			3,15 mm > P > 1 mm	—
			P < 1 mm	—
Granulometria / Particle size distribution (ISO 17827-2:2016) (1)				
Massa total analisada / total mass of test portion	—	g	P > 3,15 mm	—
Diferença entre massa da amostra e massa total das frações / / Difference mass of test portion and mass of all fractions	—	% (m/m)	3,15 mm > P > 2,8 mm	—
			2,8 mm > P > 2,0 mm	—
			2,0 mm > P > 1,4 mm	—
Humidade da amostra peneirada / Moisture content of the sieved sample	—	% (m/m)	1,4 mm > P > 1,0 mm	—
			1,0 mm > P > 0,5 mm	—
			0,5 mm > P > 0,25 mm	—
			P < 0,25 mm	—

Os resultados apresentados referem-se exclusivamente à amostra ensaiada.

iq - tal qual recebida / ar - as received; bs - base seca / d - dry basis

LQ - Limite de quantificação

(1) Ensaio não acreditado

(2) Ensaio subcontratado a laboratório com método acreditado

(3) Ensaio subcontratado a laboratório com método não acreditado

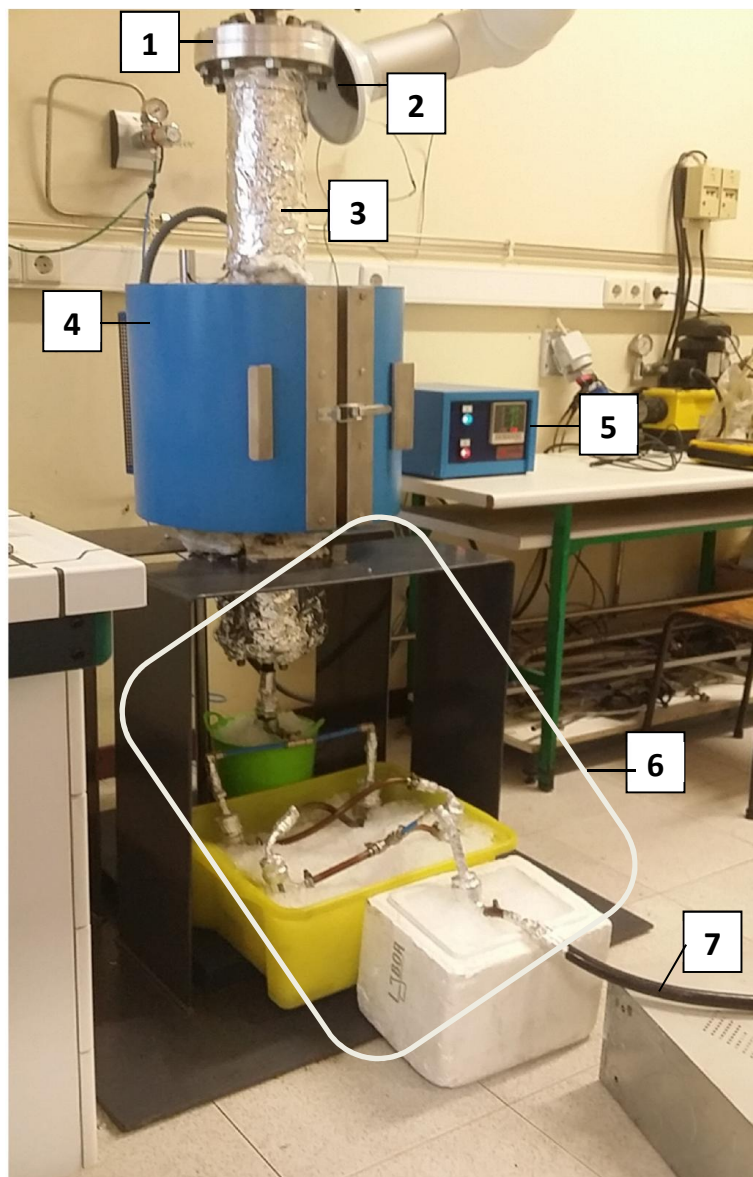
(4) Os resultados podem vir afetados pelas condições inadequadas em que a amostra foi rececionada

X *Claudia*

Cláudia Mendes
Responsável do Laboratório

Figure B.1: Results of the ultimate analysis from Centro da Biomassa para a Energia.

APPENDIX C: PHOTOGRAPHS OF THE REACTION SYSTEM



- 1 – flange connection
- 2 – exhaust hood
- 3 – steel pipe
- 4 – furnace
- 5 – temperature controller
- 6 – condensing unit
- 7 – silica gel column

Figure C.1: Reaction system.

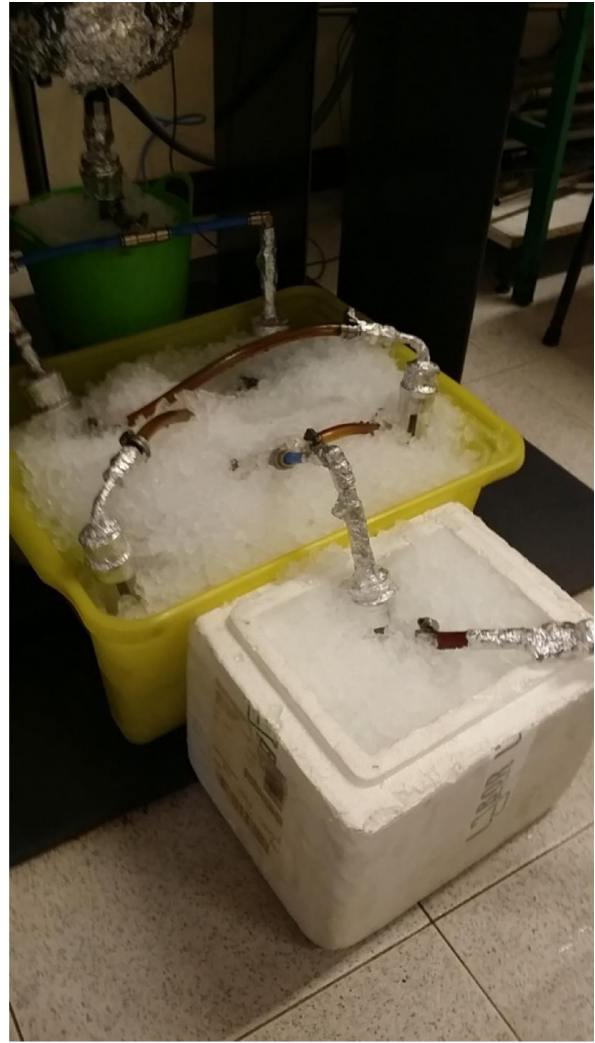


Figure C.2: Photographs of condensing system.

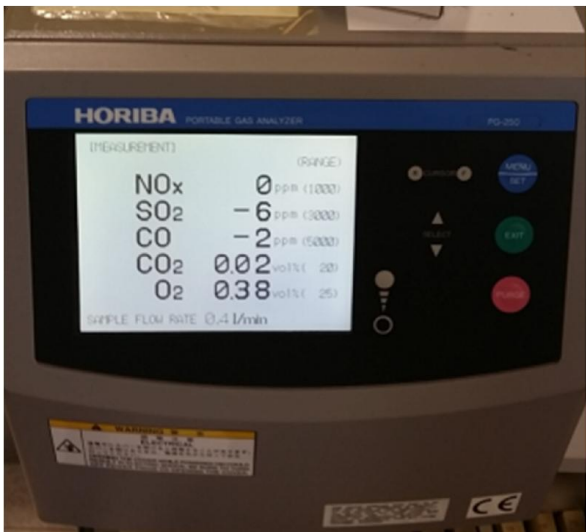


Figure C.3: Gas analyser (left) and temperature controller(right).